frontiers in Earth Science

ORIGINAL RESEARCH
published: 08 May 2018
doi: 10.3389/feart.2018.00049

Constrained Magnetostratigraphic Dating of a Continental Middle Miocene Section in the Arid Central Asia

Verena Verestek[1]*, *Erwin Appel*[1], *Silke Voigt*[2] and *Konstantin Frisch*[2]

[1] Department of Geosciences, University Tübingen, Tübingen, Germany, [2] Institute of Geosciences, Goethe University Frankfurt, Frankfurt, Germany

The Neogene succession of the Aktau Mountains in the Ili Basin, southeast Kazakhstan, is a terrestrial archive well suited for researching the role of Central Asia in Miocene climate evolution. We present an integrated approach for dating the well-exposed Bastau Formation, based on magnetostratigraphy and constraints from cyclostratigraphy and biostratigraphy. Stepwise demagnetization yielded characteristic remanence directions that are consistent with those expected for the Miocene in Central Asia. The reddish-colored alluvial floodplain deposits and gray lacustrine deposits show partly complex magnetic behavior with magnetite and hematite as the main magnetic carriers, with variable demagnetization behavior and non-dipolar normal and reverse polarity directions. The observed magnetic properties are best explained by depositional variability and magneto-mineralogical alteration effects of both dissolution and neo-formation of magnetite, including significant secondary magnetization. The mean of reverse polarity directions is flatter than the expected Middle Miocene Earth magnetic field, which is an indicator for the existence of inclination shallowing that supports a primary origin. Detailed rock magnetic analyses are used to analyze the nature of the characteristic remanent magnetization and to discriminate primary and secondary remanence directions in order to obtain a reliable magnetostratigraphic result. The proposed age of 15.3–13.9 Ma for the Bastau Formation corresponds to the known biostratigraphic setting, matches with typical sedimentation rates of foreland basins in Central Asia, and coincides with spectral analysis of geochemical proxies of that section. The resulting age model serves as a robust framework for paleoclimate reconstruction of Neogene climate dynamics in Central Asia.

Keywords: magnetostratigraphy, Miocene, paleoclimate, rock magnetism, sedimentary rocks

OPEN ACCESS

Edited by:
Kenneth Philip Kodama, Lehigh University, United States

Reviewed by:
Anne-Christine Da Silva, University of Liège, Belgium
Josep M. Pares, National Research Center on Human Evolution, Spain

***Correspondence:**
Verena Verestek
verena.verestek@uni-tuebingen.de

Specialty section:
This article was submitted to Geomagnetism and Paleomagnetism, a section of the journal Frontiers in Earth Science

Received: *05 October 2017*
Accepted: *16 April 2018*
Published: *08 May 2018*

Citation:
Verestek V, Appel E, Voigt S and Frisch K (2018) Constrained Magnetostratigraphic Dating of a Continental Middle Miocene Section in the Arid Central Asia. Front. Earth Sci. 6:49. doi: 10.3389/feart.2018.00049

INTRODUCTION

Central Asia's climate dynamics during the Cenozoic, with a general trend of aridification (Guo et al., 2002; Tang et al., 2011; Caves et al., 2015), was mainly driven by global cooling and uplift of the Tibetan plateau (Zhisheng et al., 2001; Lu et al., 2010; Miao et al., 2012). The extent of the Paratethys, together with its advance and retreat largely influenced the atmospheric moisture supply in Central Asia (Fluteau et al., 1999; Bosboom et al., 2011). To investigate these influencing factors, we study a

well-exposed paleoclimatic archive, the Neogene sedimentary succession in the Aktau Mountains (SE Kazakhstan). A robust age model that allows detailed correlation to trans-regional and global tectonic and climatic processes during the Neogene is fundamental for paleoclimatic interpretation of the proxy record. Several biostratigraphic studies provide a first rough temporal framework for the succession (e.g., Kordikova and Mavrin, 1996; Dzhamangaraeva, 1997; Lucas et al., 2000). However, the paucity of index fossils and lack of volcanic horizons compromise a detailed age model for the Aktau Mountains.

Sedimentary rocks and sediments can provide high-quality continuous magnetic polarity records contributing to the understanding of environmental processes. The source and primacy of the magnetic minerals in the sedimentary deposits are crucial for paleomagnetic studies. Secondary magnetic overprints due to viscous remanences, new formation of magnetic minerals and magneto-mineralogical alteration associated with burial, diagenesis, exhumation and exposure may complicate the analysis of characteristic remanences. Magnetostratigraphic dating of continental sediments is often more complex than for marine sequences due to a highly variable lithology causing varying rock magnetic properties, alteration and remagnetization processes (Hounslow and Nawrocki, 2008; Roberts et al., 2010; Kodama, 2012). However, under favorable conditions, one can link lithologic variations to cyclic variations in the depositional environment, i.e., precession, obliquity and eccentricity (Hays et al., 1976; Olsen and Kent, 1996; Kodama and Hinnov, 2015). Use of other approaches such as biostratigraphy and cyclostratigraphy can help to substantiate complex magnetostratigraphic dating (Krijgsman et al., 1995; Hu et al., 2005; Abels et al., 2010; Herb et al., 2015).

The studied section largely consists of red beds. Albeit the controversy on the reliability of red beds (Butler, 1992), previous studies show that red beds can carry a reliable primary detrital remanent magnetization (Tauxe et al., 1980; Tauxe and Kent, 1984; Krijgsman et al., 1999; Kruiver et al., 2003). Red beds might not be good recorders of precise paleo-remanence directions due to syn-depositional effects as inclination shallowing, but they can acquire and preserve a primary remanence and are thus a promising target lithology for recording the polarity of the Earth magnetic field. Because of the possible influencing factors mentioned above, it is essential to verify the reliability of each red bed record. Fold tests and reversal tests can yield important information about the timing of remanence acquisition and possible remagnetization processes. Moreover, rock magnetic methods are necessary to investigate remanence stability, the origin of the natural remanence magnetization and to identify possible secondary magnetizations (Kodama, 2012).

The Neogene is a period of frequent magnetic polarity reversals favoring a magnetostratigraphic approach to develop a detailed age model for the Aktau succession. In this paper, we present a detailed magnetostratigraphy of the Bastau Formation (Fm) as a fundamental basis for better understanding the Neogene climate dynamics in Central Asia. The Bastau Fm, with its depositional variability and magneto-mineralogical alteration effects, is an example of a complex continental setting. Detailed rock magnetic analyses, together with other constraints such as geochemical and cyclostratigraphic results, are required to develop a reliable temporal framework.

GEOLOGICAL SETTING

The studied succession is located in the Aktau Mountains situated in the Ili Basin, a triangular foreland basin in southeast Kazakhstan (44°00′20.3″N 79°14′40.9″E, **Figure 1**). A semi-arid desert, steppe vegetation and the Ili River dominate the today's landscape. The basin is surrounded by the foothills of the Dzhungarian Alatau Mountains to the north and the foothills of the Tien Shan Mountains to the south.

The Aktau Mountains provide an exceptionally well-exposed, long and continuous succession of Cenozoic sediments. They result from an asymmetrical anticline with a gently dipping northern flank mainly comprising lake deposits and mudflats. Bedding is fairly constant throughout the section with an average dip direction of 314° and dip angle of 10°. We did not identify any sedimentary unconformity as cemented surfaces or abrupt changes in grain size, which suggests that the sedimentary sequence is relatively continuous.

The Neogene stratigraphy of the 1,500 m-thick Aktau succession is divided into five formations (**Figure 2**; Voigt et al., 2017). Fluvial sandstones of a meandering river (Aidarly Fm) are overlain by cyclically bedded mudflats with sheet-flood deposits and paleosols (Bastau Fm). Higher up, the succession grades into ephemeral playa lake deposits (Koktal Fm), and perennial lacustrine limestones and marls (Kokterek Fm). The overlying Ili Fm roughly resembles the underlying Kokterek Fm but with more organic rich horizons (Bodina, 1961; Voigt et al., 2017). Biostratigraphic data provide a low resolution temporal framework that is useful as age marker for magnetostratigraphic dating of the Aktau Mountains (**Figure 2C**). The plant and mammal fossils (rodents, *Gomphotherium*, *Stephanocemas* and *Lagomeryx*) found at the top of the Aidarly Fm were correlated to the European mammalian biozones MN4-MN5 (Kordikova and Mavrin, 1996; Lucas et al., 1997, 2000; Kordikova, 2000; Kordikova and de Bruijn, 2001). Charophytes and the occurrence of the gomphotere *Anancus avernensis* in the lower Ili Fm suggested a Pliocene age (Bazhanov and Kostenko, 1961; Dzhamangaraeva, 1997). Accordingly, the Bastau Fm is of late Early to Middle Miocene age.

The lithology of the 90 m-thick Bastau Fm can be divided into three lithofacies based on water availability, with smooth transition between facies: alluvial fan, dry mudflat and wet mudflat (Voigt et al., 2017). The alluvial fan facies is characterized by unbedded, reddish or grayish bleached sandstone. Massive red (sandy) mudstones with occasional calcretes are typical for the dry mudflat facies. The wet mudflat facies is represented by reddish, yellow and greenish, mostly layered sandy and silty marls, often with color mottling. Additionally, with the occurrence of displacive gypsum, an increasing salinization above 55 m is observed, indicating high evaporation rates (Voigt et al.,

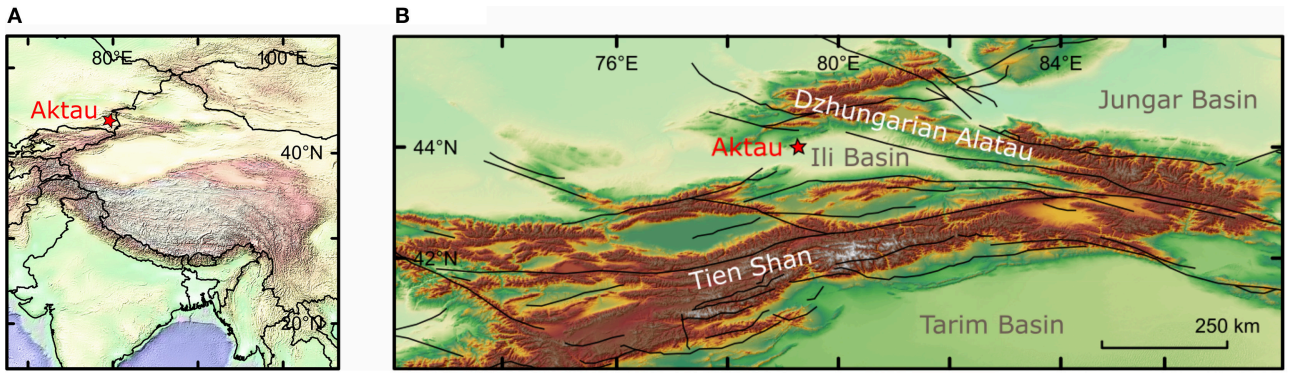

FIGURE 1 | (A) Overview map of Central Asia and the Tibetan Plateau (red star marking the location of the studied Aktau Mountains), **(B)** topographic map of the Ili Basin and the Tien Shan belt with major fault zones after Jolivet et al. (2010).

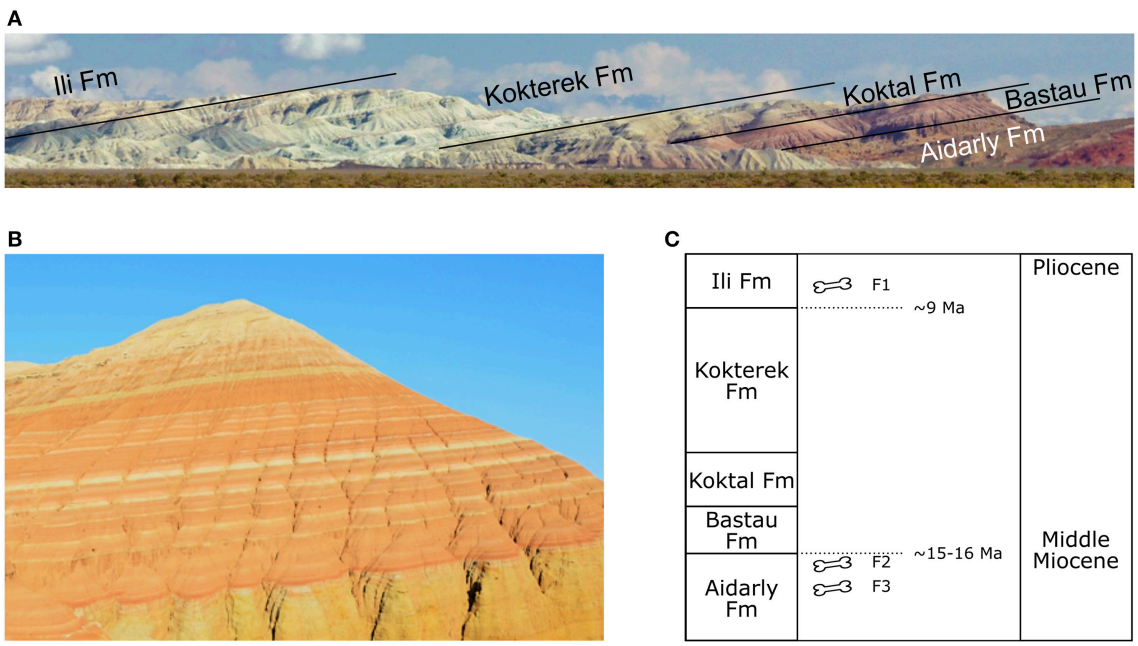

FIGURE 2 | (A) Cenozoic succession of the Aktau Mountains with the stratigraphic formations after Voigt et al. (2017), **(B)** image of the 90 m-thick Bastau Fm with the dominant red siltstones (photo by J. Pross), **(C)** biostratigraphic overview with marker fossil records: F1 after Bazhanov and Kostenko (1961), and Dzhamangaraeva (1997), F2 and F3 after Lucas et al. (1997).

2017). Further details on the lithology and facies including a detailed facies zone matrix is in progress.

SAMPLING AND METHODS

The studied sequence is characterized by small-scale heterogeneities along the sequence. Lithological heterogeneities exist even at the same stratigraphic level (e.g., small-scale variation of mottled parts), equally pronounced as between neighboring sampling levels. Thus, a dense sampling scheme was preferred over site-level sampling to ensure consistency by checking subsequent samples along the sequence. After removing the weathered surface layer, we collected samples from 503 levels (one sample per level) from fresh rock along the entire Bastau Fm. We applied a dense sampling scheme with a mean of ca. 20 cm distance between sampling levels, and partly prepared twin specimens for testing different demagnetization procedures. For sampling, we used a battery driven drill or a double-blade cutter. Drilled cylindrical samples (2.5 cm in diameter) were cut into standard specimens of 2.2 cm sides; cut samples were prepared into cubes of 2.2 cm sides. Since the content of clay is very high in all samples, we used a cordless compressor for air drilling instead of water flushing. The samples were oriented with a magnetic compass and an inclinometer.

All magnetic parameters were measured in the laboratory of Tübingen University. Full vector magnetization measurements

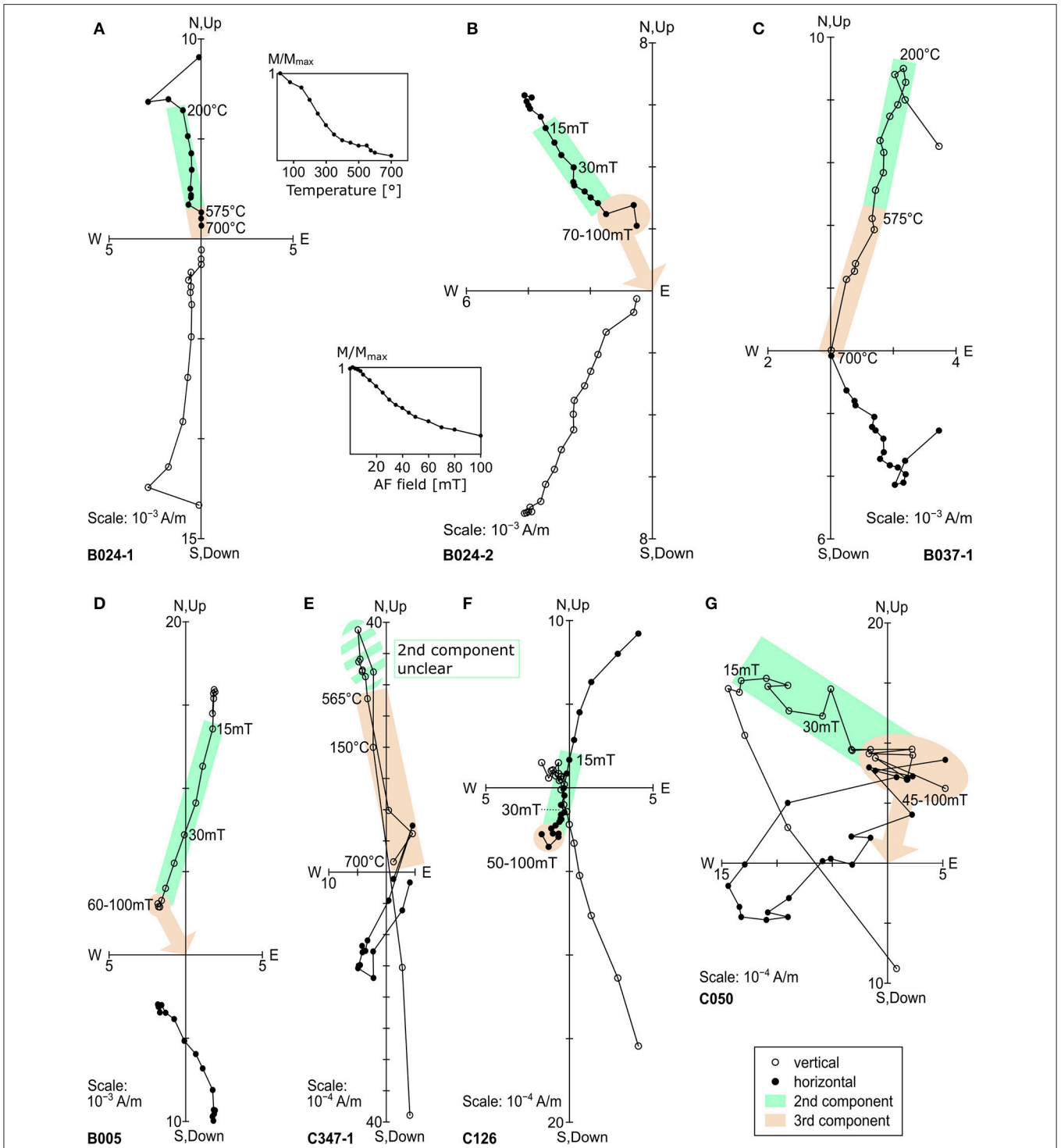

FIGURE 3 | Orthogonal end-vector projections of thermal and alternating field demagnetization data (stratigraphic coordinates) for representative samples from the Bastau Fm. Sample names are in bold. The determination of the second and third components is demonstrated in green and red (first component removed below 15 mT or below 200°C not marked). For the third component, clustering directions at high AF steps are forced to the origin (arrows, in F omitted for clarity).

of stepwise demagnetization of natural remanent magnetization (NRM) were performed on a 2G Enterprises DC-SQUID magnetometer. Alternating field (AF) demagnetization was applied in steps of 3 mT up to 45 mT and then in progressively larger steps up to 100 mT. For thermal (TH) demagnetization, the specimens were consecutively heated to temperatures

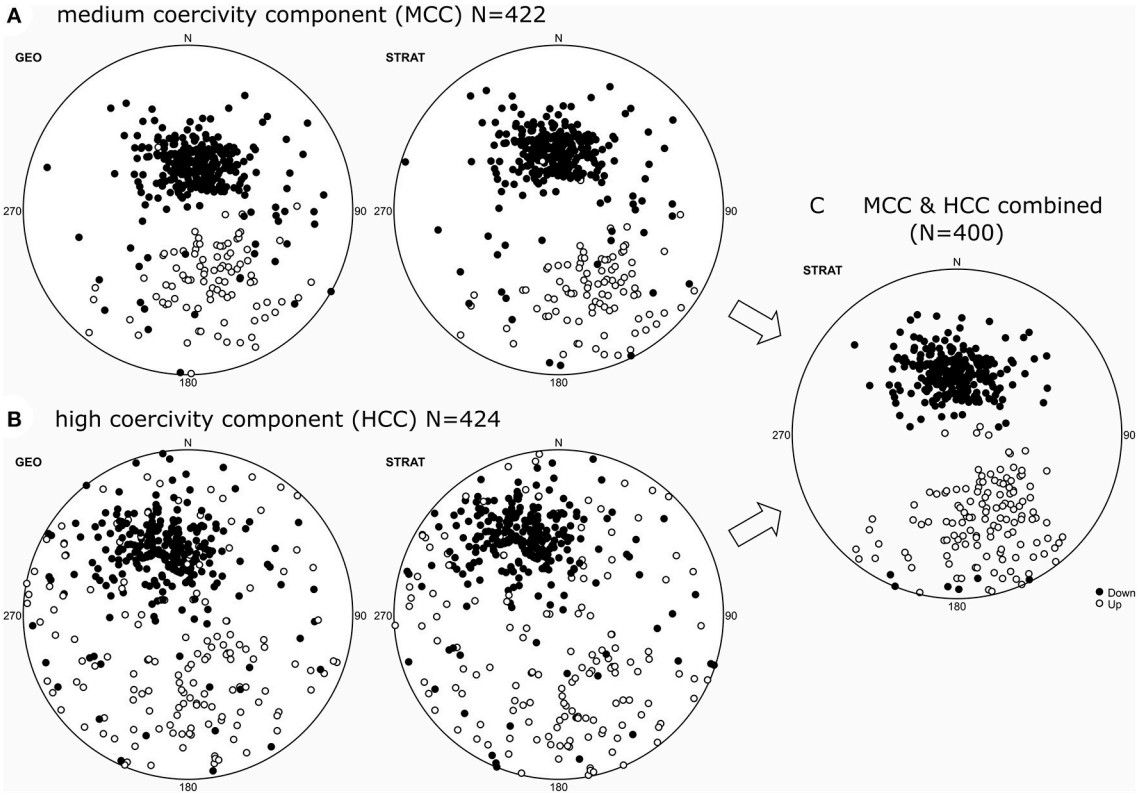

FIGURE 4 | Equal area projections of remanence directions determined from NRM demagnetization in geographic (left) and stratigraphic (middle) coordinates: **(A)** medium coercivity component (MCC) and **(B)** high coercivity component (HCC); **(C)** MCC & HCC combined data set in stratigraphic coordinates obtained from A and B (see text in section Characteristic Remanent Magnetizationfor explanation).

between 100 and 700°C in steps of 50°C (plus one step at ∼570°C). For remanence analysis from the demagnetization path we used principle component analysis (Kirschvink, 1980). For determining the high coercivity component and high temperature component the directions are forced through the origin. Mean directions of remanence populations were calculated by Fisher statistics (Fisher, 1953).

Anhysteretic remanent magnetization (ARM) was produced and measured using the SQUID magnetometer with an integrated degausser, applying a 100 mT peak alternating field and a biasing 50 μT direct field. Isothermal remanent magnetization (IRM) was imparted with a Magnetic Measurements PM9 pulse magnetizer and IRM intensity was measured with a Molspin spinner magnetometer. The IRM acquired in a 1.0 T field is taken as saturation IRM (SIRM). From SIRM and reverse IRM in a −300 mT field we calculated the high-coercivity IRM (HIRM) and the s-ratio (after Bloemendal et al., 1992). For selected samples we obtained full IRM acquisition curves (28 steps from 10 mT to 2.8 T), and decomposed the curves by log-Gaussian analysis after Kruiver et al. (2001) in order to characterize the different ferro(i)magnetic phases by their medium acquisition field ($B_{1/2}$) and to determine their contribution to the IRM signal.

Susceptibility measurements were performed with an AGICO MFK1-FA Kappabridge. Bulk susceptibility expressed in mass-specific units (χ) and its frequency dependence (kfd) were determined from bulk samples at two different operating frequencies (976 Hz and 15,616 Hz). High-temperature susceptibility runs were done by heating sample powder (∼0.2 g) to 700°C in air at low heating rate (11°C/min) and measuring susceptibility during the full heating and cooling cycle. Anisotropy of susceptibility (AMS) was measured with a 3D-rotator and analyzed in volume-specific units (k). AMS parameters P_j and T (Jelinek, 1981) were calculated to describe the degree of anisotropy and the shape of the AMS tensors. Hysteresis loops were obtained on small sub-samples (∼2 mg) with a PMC MircoMag 2900 (max. field 500 mT), extracting the ratios of saturation remanence to saturation magnetization (M_{rs}/M_r) and coercivity of remanence to coercivity (H_{cr}/H_c).

PALEOMAGNETIC AND ROCK MAGNETIC RESULTS

Remanence Analysis

A subset of 10 samples (each one divided into twin specimens) was chosen as pilot samples and subjected

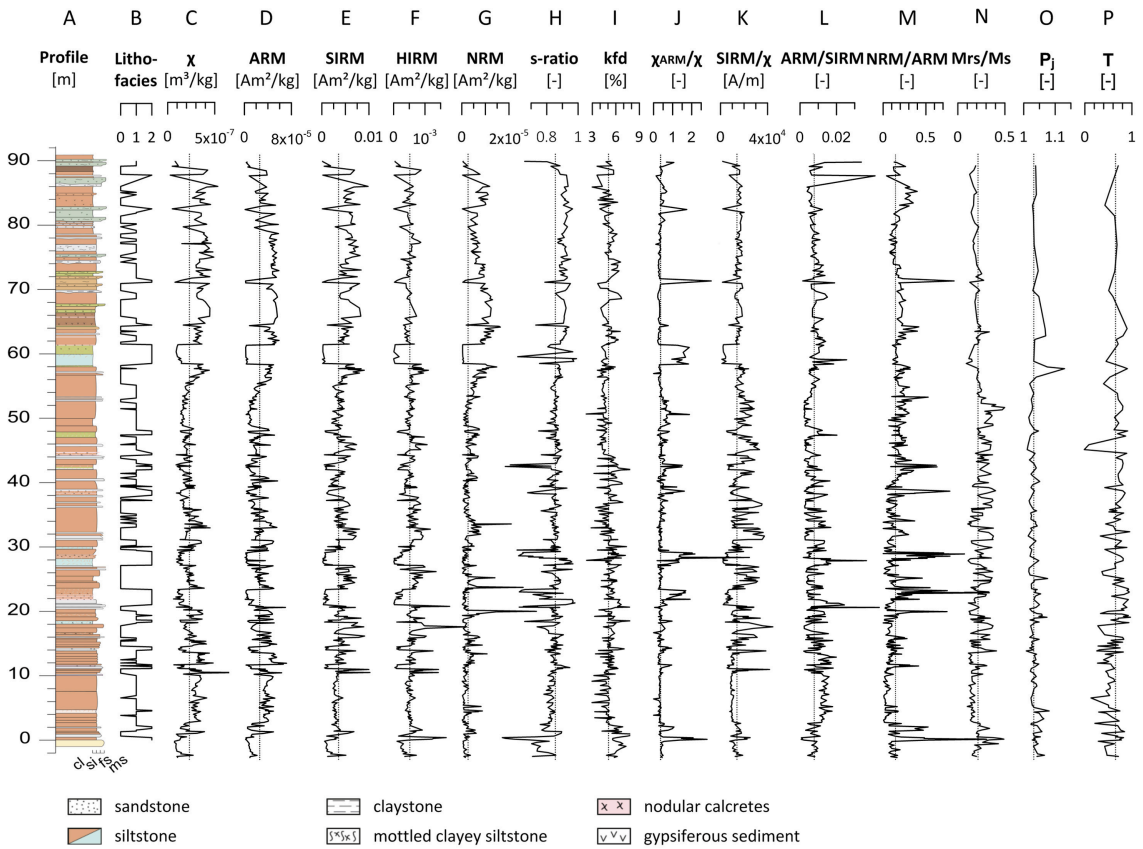

FIGURE 5 | Rock magnetic parameters measured along the section with median values indicated by dashed lines: **(A)** profile with simplified color chart and grain size indication on the right (cl, claystone; si, siltstone; fs, fine sandstone; ms, medium sandstone), **(B)** lithofacies (0–alluvial fan, 1–dry mudflat, 2- wet mudflat), **(C-G)** concentration-dependent parameters (χ, SIRM, ARM, HIRM, NRM), **(H)** magnetic mineral indicator (s-ratio), **(I-L)** grain size dependent ratios (kfd, χ_{ARM}/χ, SIRM/χ, ARM/SIRM), **(M)** NRM/ARM as an indicator for natural remanence intensity to remanence capacity, **(N)** magnetic grains size (i.e. domain-state) indicative ratio M_{rs}/M_s, **(O,P)** parameters of degree and shape of anisotropy of magnetic susceptibility (P_j, T). For explanation of abbreviations, see section Sampling and Methods.

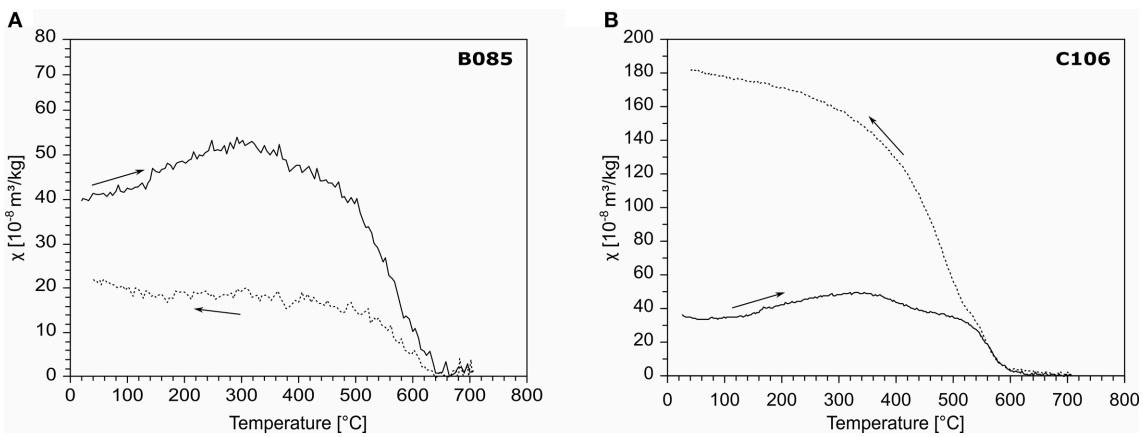

FIGURE 6 | Bulk susceptibility vs. temperature curves of representative samples of the Bastau Fm. Both curves show the typical decrease around 580°C, corresponding to the Curie temperature of magnetite, and non-reversible behaviors; in **(A)** magnetite is destroyed at high temperature whereas in **(B)** new magnetite is produced.

to AF and TH demagnetization. AF demagnetization adequately resolved magnetic components for samples from all lithologies, and we thus chose AF treatment as the standard demagnetization procedure for the bulk of the specimens. In total, 503 specimens were treated with AF demagnetization. For control, additional 73 specimens

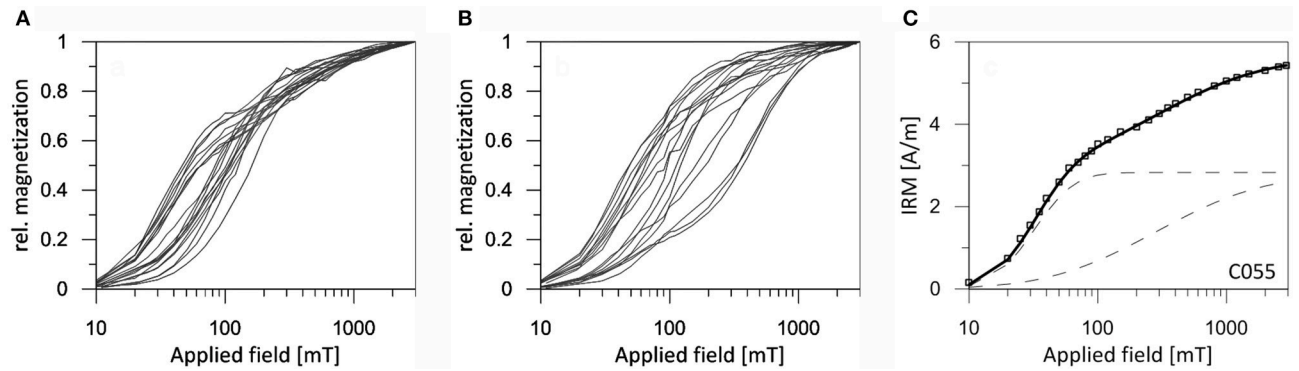

FIGURE 7 | Isothermal remanence magnetization acquisition curves: **(A)** alluvial fan and dry mudflat facies types, **(B)** wet mudflat facies type, **(C)** end member modeling for sample C055 (dry mudflat facies type) after Kruiver et al. (2001) with the two end member components magnetite and hematite indicated with dashed lines.

(twin specimens from same levels) were analyzed with TH demagnetization.

Both AF and TH demagnetization yield similar results (e.g., twin specimens of sample B024 in **Figures 3A,B**). The majority of specimens show three components of remanent magnetization. The remanence removed at low AF fields <15 mT or at low temperatures <200°C shows highly scattered direction with a slight tendency toward the present Earth magnetic field direction. This soft magnetic or viscous remanence will not be further discussed. A medium coercivity component (MCC) is isolated using AF demagnetization data from 15 to 30 mT or higher. At the maximum AF field (100 mT) the specimens are not completely demagnetized. The residual remanence from 60 to 70 mT onward shows relatively constant intensities and clustering remanence directions, which are predominantly quite stable (**Figures 3D,F**), though partly also noisy cases occur (**Figure 3G**). This residual remanence indicates a high coercivity component (HCC) which is immune against AF demagnetization. It can only be demagnetized to the origin by TH treatment. However, a more detailed analysis of the final (TH) demagnetization path is not possible because of the relatively low intensity of the residual remanence compared to the NRM intensity (**Figures 3B,D,F**). As a reasonable approximation of the HCC, we determined its direction by averaging the clustering residual directions anchoring them to the origin. TH demagnetization results give a hint about the remanence carriers. Most of the NRM is unblocked below 600°C, but part of it survives until temperatures between 600 and 700°C (**Figures 3A,C,E**). This points out that magnetite and hematite are the likely carriers of the MCC and HCC, respectively.

For most specimens, the MCC and HCC show directions of the same polarity. However, for 7% of the samples, the HCC exhibits a reverse polarity direction while the MCC indicates a normal polarity direction (**Figure 3F**). The contrary, i.e., a reverse polarity MCC paired with a normal polarity HCC, never occurs. **Figure 4** displays the dispersions of all extracted remanence directions of the MCC (**Figure 4A**) and HCC (**Figure 4B**) in separate plots. Both components show roughly antipodal remanence directions, and thus are potential

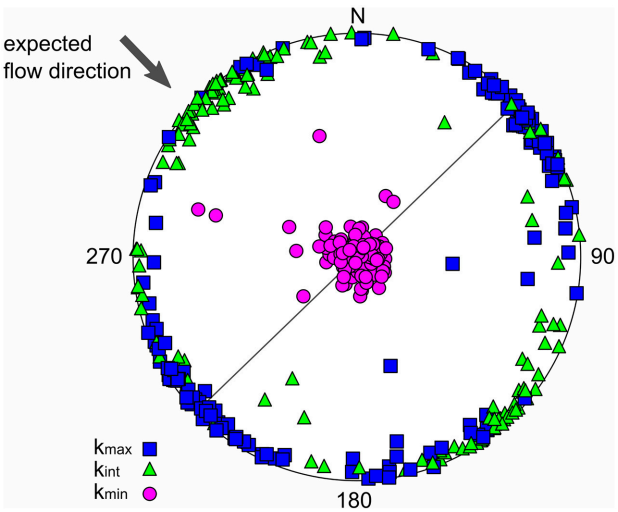

FIGURE 8 | Anisotropy of susceptibility principle axes (tilt-corrected coordinates): minimum principle axes (k_{min}, circles) group perpendicular to the bedding plane, maximum principle axes (k_{max}, squares) group in the strike direction (gray line) of the bedding plane.

carriers of a characteristic paleo-remanence. The HCC scatters much more than the MCC, which is likely due to the approximative determination of this component. Normal and reverse polarity directions of the HCC tend to be antiparallel (normal polarity mean D/I = 334.0°/41.4°, reverse polarity mean D/I = 171.2°/−48.8°) and both polarity directions show relatively similar scatter, whereas for the MCC the normal polarity directions (mean D/I = 355.8°/62.5°) are clearly steeper and more clustered than the reverse polarity directions (mean D/I = 155.7°/−40.5°).

Magnetic Mineralogy

Rock magnetic properties provide further information on the stability and the origin of magnetic remanences. Below, we separate these results into their indication for magnetic

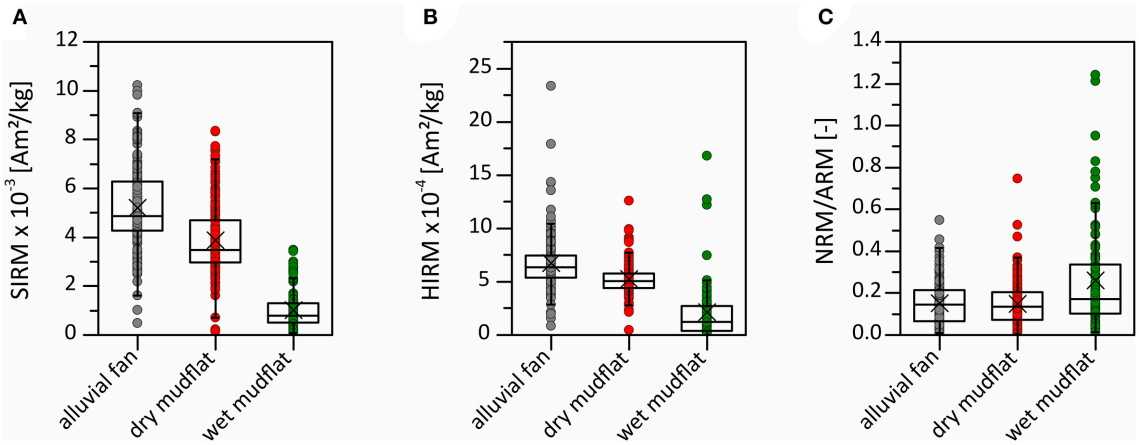

FIGURE 9 | Lithofacies and rock magnetic characteristics: box plots of the concentration-dependent parameters **(A)** SIRM, **(B)** HIRM, and **(C)** NRM/ARM ratio with means indicated by crosses, quartiles boxes and whiskers with a factor of 1.5. All consistently indicate statistically different mean values for the wet mudflat facies, supporting alteration of the primacy magnetic mineralogy in this facies.

concentration, magnetic mineral type, magnetic grain-size, and magnetic fabric.

Concentration-Dependent Parameters

The concentration-dependent magnetic parameters vary with lithology. Bulk magnetic susceptibility χ (**Figure 5C**) shows an increase above 55 m. Samples from the alluvial fan and dry mudflat facies show higher values than wet mudflat samples. A similar pattern is observed for the intensities of ARM (**Figure 5D**), SIRM (**Figure 5E**) and NRM (**Figure 5G**). Also HIRM values (**Figure 5F**) are lower in the wet mudflat facies; however, there is no increase above 55 m.

Magnetic Minerals

Temperature dependent results suggest the existence of at least two magnetic phases in all lithologies of the Bastau Fm. In all studied samples, a marked decrease around 550–580°C is seen in high-temperature susceptibility runs, which clearly reveals the presence of magnetite (**Figure 6**). Most samples show a decrease around 350–450°C which can be attributed to the inversion of maghemite to hematite. Hematite is not observed in the thermomagnetic curves as the presence of magnetite overrides its very low susceptibility. In most samples, strongly enhanced values appear in the cooling curves accompanied by a continuous increase during cooling (**Figure 6B**). We explain this observation with new formation of ultrafine superparamagnetic magnetite particles (with a range of different grain sizes) at high temperatures during heating, which transform from the fully unblocked state to the state of higher susceptibility during cooling (Bowles et al., 2009). The new formation of magnetite during heating is more pronounced in the mudflat layers.

The s-ratio (**Figure 5H**) varies between 0.52 and 0.99 (median 0.86) implying a high fraction of hematite in most of the samples. Like the concentration-dependent parameters, s-ratios change above 55 m, showing higher values in the upper part.

Unmixing of IRM acquisition curves (Kruiver et al., 2001) for representative samples of all three facies types (**Figures 7A,B**, in total 28 samples) indicate the presence of both magnetite and hematite. The lower coercivity end member component has mean $B_{1/2}$-values between 30 and 100 mT, which can be related to magnetite. This first end member component has relatively lower $B_{1/2}$-values for alluvial fan and dry mudflat samples compared to wet mudflat samples. The $B_{1/2}$-values of the second end member component varies between 100 and 700 mT, which according to maximum unblocking temperatures during TH demagnetization of the SIRM (**Figure 7C**) represents hematite. Occasionally a third end member component with $B_{1/2}$-values >1,500 mT is identified contributing <20% to the SIRM signal. This third component could be interpreted as a second hematite fraction with relatively higher coercivity. Contributions of goethite can be excluded based on TH demagnetization of IRM. The contributions of the first and second end member components are relatively equal in the alluvial fan and dry mudflat samples. In wet mudflat samples, the contributions are more variable, with 30–90% for the first component, indicating a relatively higher magnetic fraction than in the other two facies types. Interestingly, for those samples from the wet mudflat facies showing striking color mottling, the first component either contributes relatively less to the total SIRM (<45%) with $B_{1/2}$-values around 35–75 mT, or has higher coercivities ($B_{1/2}$-values around 100 mT) contributing up to 89% to the total SIRM.

Magnetic Grain-Size Characteristics

The frequency dependent susceptibility kfd is generally low with an average value of 5% (**Figure 5I**). Thus, non-superparamagnetic grains dominate the ferro(i)magnetic mineral assemblage.

The lower values of χ_{ARM}/χ and SIRM/χ (**Figures 5J,K**) in the wet mudflat layers are likely caused by a decrease of the magnetite fraction and reflect a relatively higher paramagnetic contribution. The ARM/SIRM ratio (**Figure 5L**) is a more

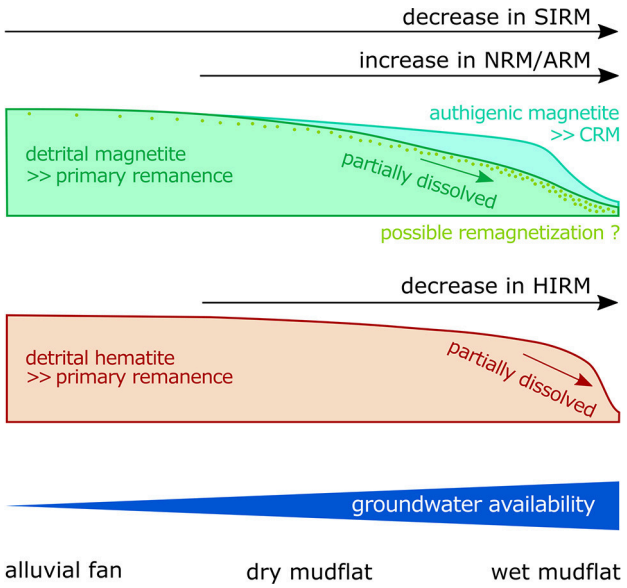

FIGURE 10 | Principle sketch of the interpreted magnetic alteration scenario of the ferro(i)magnetic phases, comprising dissolution and neo-formation of magnetite and dissolution of hematite, causing secondary chemical remanent magnetization (CRM) of authigenic magnetite and possibly also partial remagnetization of the detrital fraction.

suitable magnetic grain size indicator as it only depends on the ferro(i)magnetic phases. Its strong fluctuation between stratigraphic levels of 10 m and 50 m suggests a complex magnetic behavior in this part.

Hysteresis loops are dominated by low coercivity values, they close around maximum 300 mT, and they are not a wasp-waisted, highlighting the magnetite fraction (i.e., the existing hematite fraction is obviously hidden in these curves). The hysteresis parameters are rather variable. Saturation magnetization values (M_s) are low in samples from the wet mudflat facies and range from high to low in samples of the alluvial fan and dry mudflat facies. The magnetic grain size dependent ratios M_{rs}/M_s (**Figure 5N**) and H_{cr}/H_c do not resemble the stratigraphic pattern of the ratios χ_{ARM}/χ, SIRM/χ and ARM/SIRM. The samples used for hysteresis measurements are likely too small (2 mg) to average on the internal heterogeneity of the sediment while χ_{ARM}/χ, SIRM/χ and ARM/SIRM were obtained from larger bulk samples of several grams. The reliability of the hysteresis results is obviously limited, and thus, we omit the results of hysteresis for further interpretations.

Anisotropy of Magnetic Susceptibility

We measured the AMS of 152 samples along the Bastau Fm. **Figures 5O,P** shows changes in AMS parameters (Jelinek, 1981) with stratigraphic position. The degree of anisotropy P_j varies from 1.008 to 1.130 with an average of 1.035. The shape parameter T ranges from −0.013 to 0.969 with a mean of 0.637 and clearly indicates an oblate shape. Variations of P_j and T throughout the stratigraphic section show no relationship with the variation of the concentration-dependent parameters. The k_{max} and k_{min} principle axes (**Figure 8**) are well grouped, with a bedding parallel fabric after tilt correction. The k_{max} directions are preferentially aligned NE-SW, i.e., in the strike direction of the bedding planes, and the k_{min} directions group very well perpendicular to the bedding plane, supporting a primary sedimentary fabric.

DISCUSSION AND MAGNETOSTRATIGRAPHY

Main Magnetic Carriers and Salinity

Detailed rock magnetic analyses revealed magnetite and hematite as the main magnetic carriers in samples from the Bastau Fm. We interpret the trend of higher values of the s-ratio (**Figure 5H**) and the concentration-dependent parameters χ, ARM and SIRM (**Figures 5C,D,E**) above 55 m as an increase in the absolute magnetite content. The mean level of HIRM values (**Figure 5F**) indicates a fairly constant hematite content throughout the section, i.e., no increasing or decreasing trend. Relatively similar residual magnetization intensities after AF demagnetization also support this interpretation. Higher magnetite concentration above 55 m is likely related to lithological changes with higher groundwater levels, higher fluctuations and salinity and intensified authigenic mineral formation (Voigt et al., 2017), including possible new formation of magnetite. For this upper part, Voigt et al. (2017) propose increasing evaporation rates in a progressively hydrologic restricted basin above 50 m.

Source of Sedimentary Input

AMS has been widely used in rock magnetic studies to understand the hydrologic regime, transport and depositional conditions of sediments or tectonic effects, also in the foreland basins of the nearby Tien Shan (Gilder et al., 2001; Charreau et al., 2005; Tang et al., 2012). The distribution of the principle AMS axes (**Figure 8**) is typical for sedimentary fabric with hydromechanical and/or gravitational processes that influence the alignment of (magnetic) grains during deposition (Tarling and Hrouda, 1993; Charreau et al., 2006; Itoh et al., 2013). The clustering of k_{max} is perpendicular to the transport direction proposed by Voigt et al. (2017). Detrital sedimentary discharge, e.g., by mudflows, coming from the foothills of the Altyn Emel and Dzhungarian Alatau in the north-west likely aligned the (geometrical) long axis of particles in NE-SW direction, indicating a fast paleocurrent flow (Tarling and Hrouda, 1993; Felletti et al., 2016).

Lithofacies Dependence of Rock Magnetic Mineralogy

The contribution of the magnetic phases to the magnetic signal varies with lithofacies. All concentration-dependent parameters (**Figures 5C-G**) show lower values for the wet mudflat facies, i.e., SIRM and HIRM are highest in the alluvial fan facies and lowest in the wet mudflat facies (**Figures 9A,B**). We interpret these variations as a concentration variation of both magnetite and hematite in the samples. The concentration of ferro(i)magnetic minerals is obviously decreasing with increasing groundwater availability.

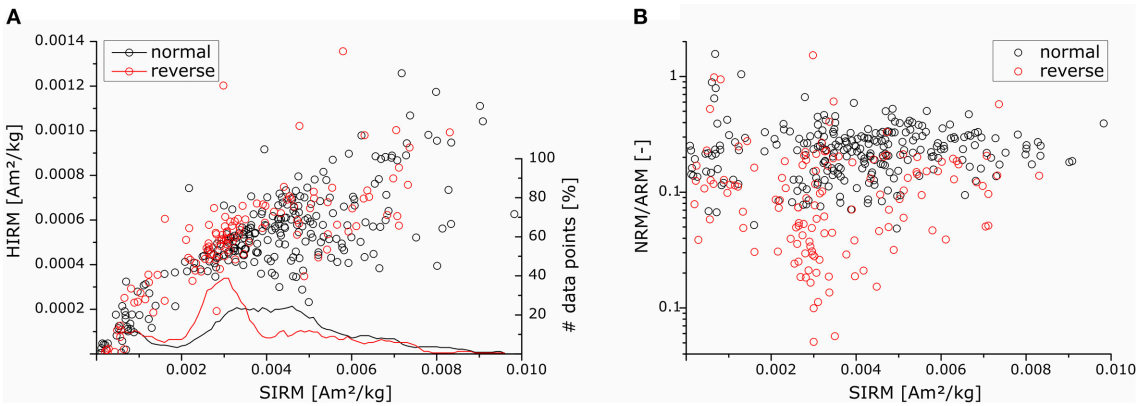

FIGURE 11 | (A) HIRM vs. SIRM and **(B)** NRM/ARM vs. SIRM scatter plots. In black (red) are the data points for samples with normal (reverse) polarity directions. The solid curves in A indicate the relative distribution of data points calculated from running means of 0.001 Am²/kg-windows for samples with normal (black) and reverse (red) polarity directions.

The three facies types are characterized by different intensities of pedogenic reworking under arid conditions evident from the neo-formation of Mg-rich clay minerals as palygorskite (Voigt et al., 2017). Authigenic mineral formation favorably occurs in the capillary fringe by evaporative groundwater rise (Deocampo, 2015) and is most pronouncedly developed in the wet mudflat facies.

New formation of magnetite during high temperature thermomagnetic runs (**Figure 6B**) is more pronounced in the wet mudflat layers. This supports the interpretation of enhanced soil formation in this facies by Voigt et al. (2017) as magnetite formation during high temperature runs is typical for soil and paleosols (Zhang C. et al., 2012; Jordanova, 2016; Sun et al., 2017).

The ratio of the NRM and ARM (**Figure 5M**) represents the natural remanence intensity (NRM) normalized to the remanence acquisition capability (given by the ARM). The NRM/ARM-ratio is higher in the wet mudflat facies and shows much higher variation in this facies type (**Figure 9C**). A higher NRM/ARM-ratio may indicate the presence of a secondary chemical remanent magnetization, which often carries a strong remanence intensity (Deng et al., 2007).

One has to note that classification of samples into the three facies types is not straightforward (see **Figure 5B** for their interpreted distribution along the section), and thus the differences of the considered rock magnetic parameters are certainly larger than indicated by the results in **Figure 9**.

Characteristic Remanent Magnetization

The time-averaged dipole field direction at the Aktau location has an inclination I = 62.6° (ambient present-day field direction: declination/inclination D/I = 4.9°/64.4°). The expected direction during the Middle Miocene calculated from the apparent polar wander path of Torsvik et al. (2012) is quite similar to the present one, i.e., D/I = 351.2°/64.4° with a corresponding virtual geomagnetic pole (VGP) at latitude/longitude = 83.4°/57.9°. The bedding planes are uniformly tilted at a low angle of 10°. Thus, recent or earlier overprints are difficult to identify and to discriminate from normal paleo-directions of primary origin.

In a first step, we combine the MCC and HCC (**Figures 4A,B**) into a common characteristic remanent magnetization (MCC & HCC combined) data set. Principle criteria for rejecting specimens are a mean angular deviation (MAD) >15°, and directions strongly deviating from the expected paleo-direction (used threshold: VGP latitude <30°). The accuracy in the determination of the MCC is usually better than for the HCC. For most specimens showing the same polarity for both components, we thus used the MCC in the MCC & HCC combined data set. Only in 54 cases for which the MCC does not meet the MAD and VGP threshold, but the HCC does, we selected the latter one. Specimens with dual polarities of both components (7 % of all samples) all show a normal polarity direction for the MCC. This indicates a secondary origin of the MCC in these samples, and we thus regarded the reverse polarity HCC as the valid paleo remanence direction (if it meets the MAD and VGP criteria). According to this procedure and the rejection criteria, 103 from the 503 sample levels were excluded.

Figure 4C shows an equal area projection of the accepted MCC & HCC combined directions consisting of 320 MCC data (236 and 84 of normal and reverse polarity, respectively) and 80 HCC data (26 and 54 of normal and reverse polarity, respectively). Reverse polarity directions show a higher dispersion than normal polarity directions, which can be explained by three reasons, all of them based on the fact that the normal polarity directions include a much higher part of the MCC than the reverse polarity directions (90 and 61%, respectively). First, the HCC often contributes relatively little to the total NRM signal, and thus its determined remanence direction (from stable end points during AF demagnetization) is noisier than for the MCC. Second, hematite particles (the likely carrier of the HCC) have a weaker magnetostatic interaction with the Earth magnetic field during their deposition. Third, the normal polarity MCC is likely contaminated to some degree by secondary chemical magnetizations, which are better clustered.

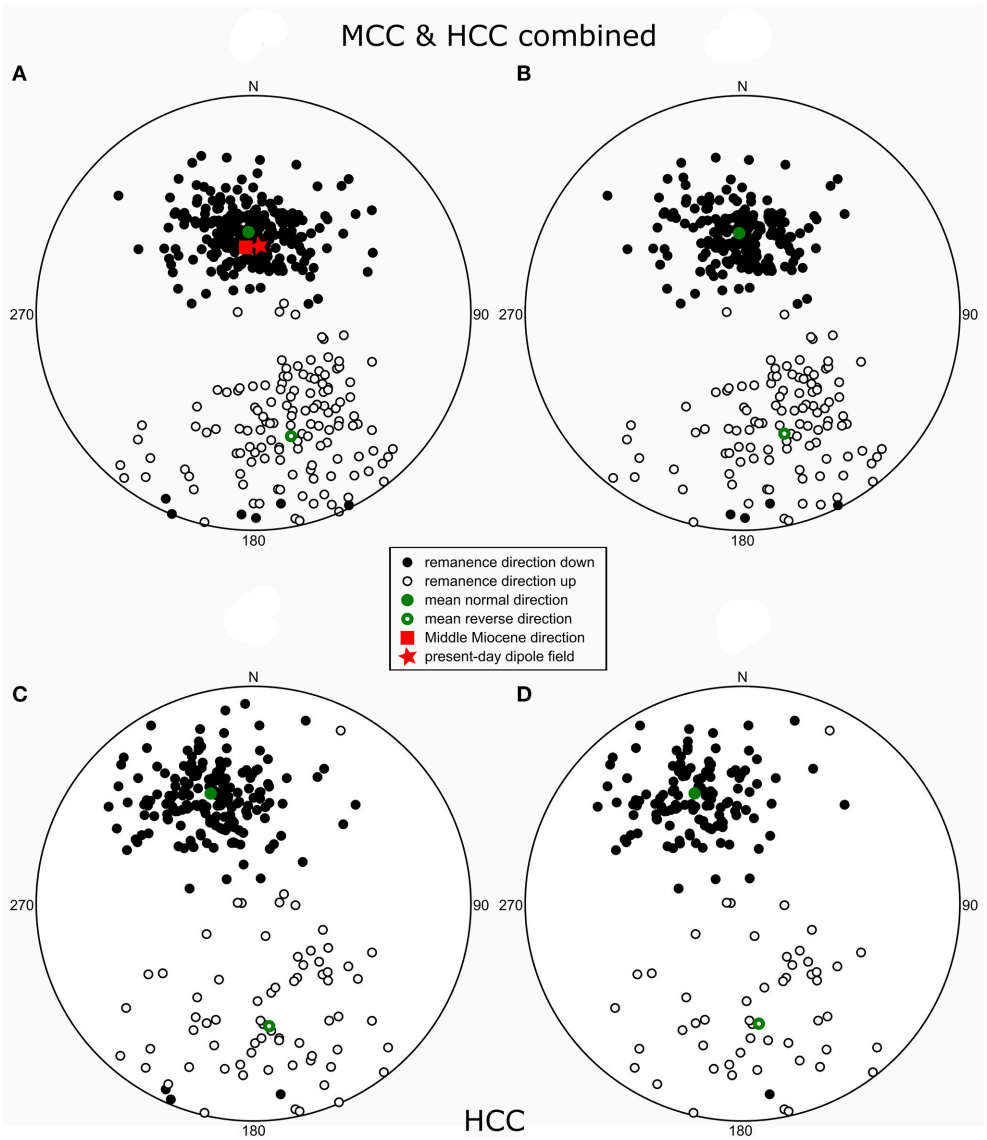

FIGURE 12 | Equal area projection of remanence directions (in stratigraphic coordinates) determined from demagnetization of NRM (mean directions of normal and reverse polarities are indicated by green circles): **(A)** directions from the MCC & HCC combined data set as shown in **Figure 4C** with expected Middle Miocene (red square) and present-day (red star) Earth magnetic field directions; **(B)** MCC & HCC combined data retained after rock magnetic selection (used for the final magnetostratigraphy; see **Figure 13E**); **(C)** HCC directions only and **(D)** HCC directions filtered by the same rock magnetic criteria.

Normal polarity directions clearly dominate the combined MCC & HCC data set. This may be due to the dominating normal polarity intervals during the time of deposition of the Bastau Fm, but also secondary magnetization effects could add to the imbalance of polarities. The interpreted alteration scenario and its possible relationship with magnetic overprinting is further discussed in the following section Magnetic Alterations and Remagnetization.

Magnetic Alterations and Remagnetization

Secondary overprinting is a common process in sedimentary rocks (McCabe and Elmore, 1989; van der Voo and Torsvik, 2012; Roberts, 2015). Transformation, low-temperature oxidation, dissolution and neo-formation could lead to changes in coercivity, e.g., due to a change of the effective particle size and inhomogeneities generated within particles (Zhang W. L. et al., 2012; Hu et al., 2015). The directions in our MCC & HCC combined data set (**Figure 4C**), particularly the normal polarity ones, are likely contaminated by secondary magnetizations due to new formation and partial remagnetization of ferro(i)magnetic phases during diagenetic processes and later alteration. Samples from the wet mudflat facies are preferred candidates for the presence of secondary magnetizations as they show lower NRM values with partially normal polarity directions in stratigraphic

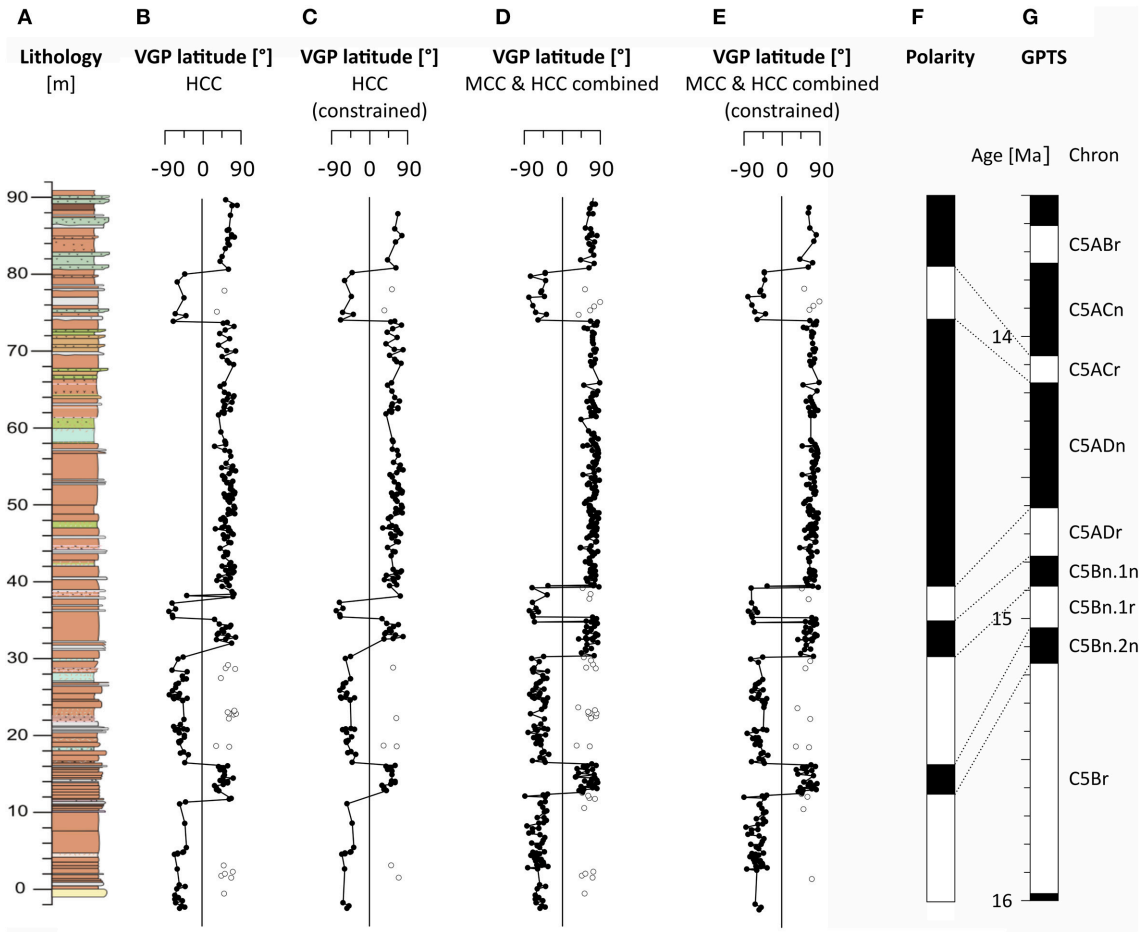

FIGURE 13 | Magnetostratigraphic results for the Bastau Fm based on the rock magnetic data-selection criteria: **(A)** stratigraphic column (as in **Figure 5A**), **(B,C)** VGP (North poles) latitude plots based on the HCC only and **(D,E)** based on the MCC & HCC combined data set (selections correspond to **Figures 12B,D**, respectively), open circles indicate still remaining questionable normal polarity directions within reverse polarity intervals (see text for further explanation), **(F)** resulting polarity pattern correlated to **(G)** the GPTS after Gradstein et al. (2012).

intervals where specimens from other facies types suggest a reverse polarity.

Chemical alteration in arid and semiarid settings responds sensitively to changes in the hydrologic system of a basin. Voigt et al. (2017) used bulk-sediment geochemistry to derive weathering indices and studied changes in the intensity of weathering and pedogenesis in the Bastau Fm. They observed elevated weathering intensities as a result of pronounced pedogenesis in periods of driest climatic conditions in settings when the regional evaporation rate was high and the alluvial sedimentary discharge was low. Elevated values of weathering indices (i.e., Mg-enrichment by authigenic formation of Mg-rich clay minerals) as well as low Ti/Al ratios occur in the wet mudflat facies, i.e., in horizons that are characterized by mottling and associated color changes from pedogenic reworking (**Figures 15A,B**). These horizons formed during times of intensified evaporation, higher groundwater table and associated capillary groundwater rise. Gale et al. (2006) attributes color mottling in clay rich sediments to repeated drying and wetting of soils and the non-uniform process of ferrous iron to ferric iron reduction. The presence of rutile in wet mudflat layers (Voigt et al., 2017) also suggests reductive conditions. Rock magnetic parameters suggest syn- and post-depositional alteration of magnetite, linked with secondary magnetic overprinting and poorer remanence conservation. The dry mudflats were deposited during periods of higher hinterland precipitation and accordingly higher detrital sediment production. These wet conditions are less seasonal with continuous sedimentary input, more stable aggradation of mudflats and pedogenesis with well drained descendent soils (Voigt et al., 2017) favoring conservation of primary ferro(i)magnetic phases.

The variations of the concentration dependent magnetic parameters with lithofacies and the different coercivities and contributions in the end-members from IRM decomposition samples of the wet mudflat facies are indicative for an alteration of the ferro(i)magnetic fraction. The wet mudflat facies is characterized by an elevated groundwater table wherefore reducing conditions are dominating the diagenesis in these

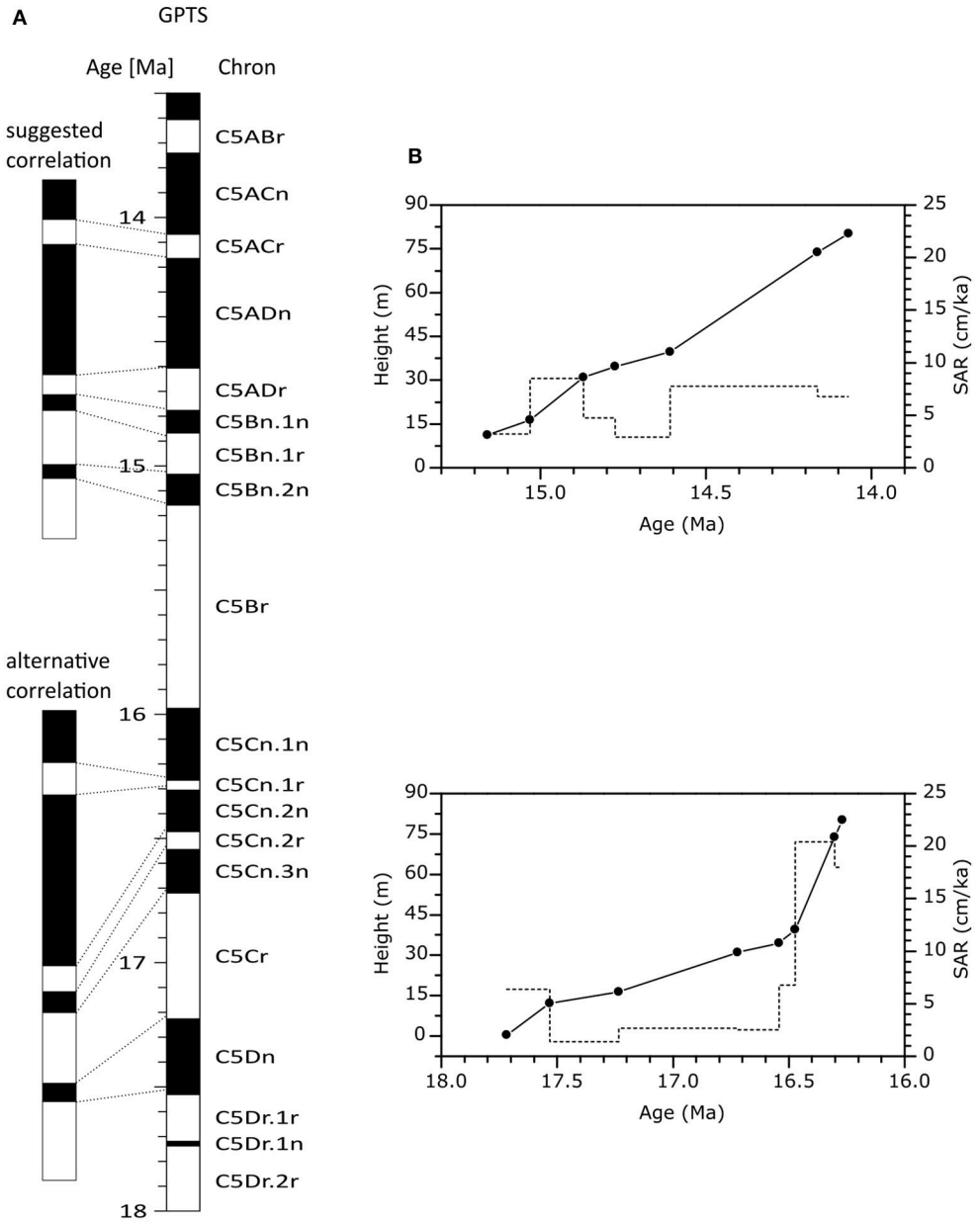

FIGURE 14 | (A) Suggested and possible alternative magnetostratigraphic correlation of the polarity pattern retrieved from the VGP latitude to the GPTS after Gradstein et al. (2012), **(B)** corresponding height vs. age plots (black line) with sediment accumulation rates (SAR, dashed line) calculated for each fully resolved chron.

horizons (Voigt et al., 2017). We propose dissolution and neo-formation of magnetite as the main alteration processes (see principle scenario in **Figure 10**), which we explain in the following paragraphs.

In the Bastau Fm the paleo-remanence is likely carried by fine and coarse magnetite and hematite grains. Multi-domain grains are susceptible to remagnetization and less effective recorders of paleo magnetizations than fine single domain grains (Butler, 1992). Certainly, remagnetization of soft magnetic particles may also be present in all facies types of the Bastau Fm (**Figure 10**).

Magnetite dissolution has been studied in laboratory experiments (Karlin and Levi, 1985; Canfield and Berner, 1987) and found to have profound influence on remanence stability (Roberts et al., 2013). Dissolution of magnetite is well known from water-logged sediments (Florindo et al., 2003; Demory et al., 2005; Taylor et al., 2014). Partial dissolution of magnetite in the Bastau section is indicated by lower concentration-dependent values (**Figures 5C,D,E**), and a decrease of the χ_{ARM}/χ and SIRM/χ ratios (**Figures 5J,K**) that is likely related to a stronger contribution of paramagnetic minerals to χ. The proposed dissolution process, which most affected the

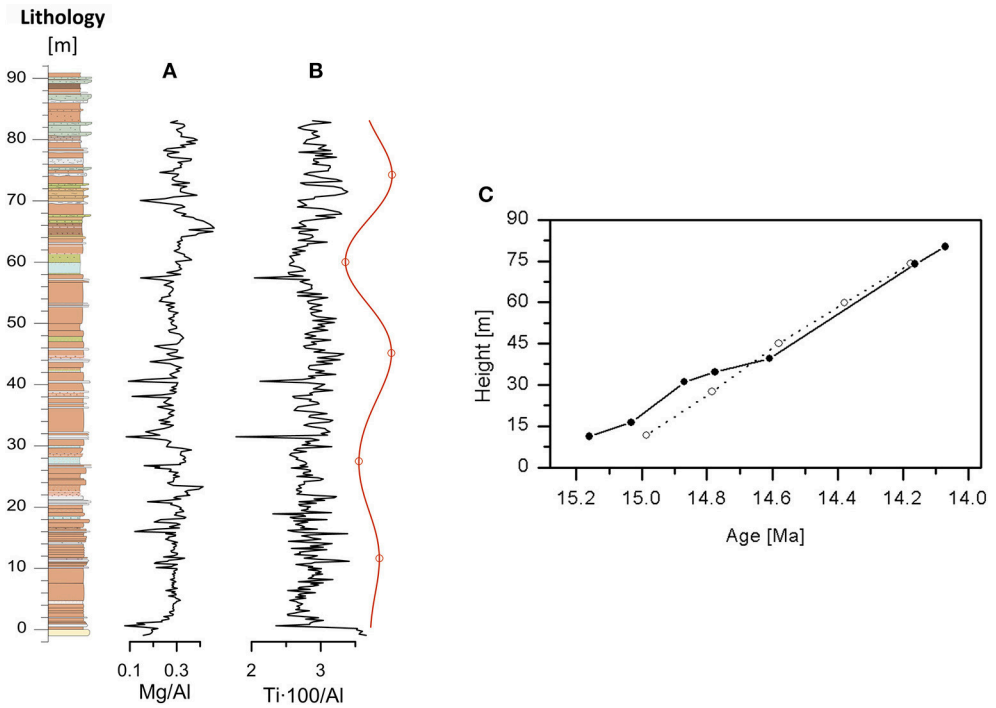

FIGURE 15 | Geochemical proxies along the profile (as in **Figure 5A**): **(A)** Mg/Al ratio and **(B)** Ti/Al ratio with long eccentricity filter output in red (both from Voigt et al., 2017), and **(C)** height vs. age correlation from magnetostratigraphy (black line) and time-series analysis of the Ti/Al ratio (dotted).

wet mudflat facies, likely dissolved the magnetite particles partially (**Figure 10**), shifting the magnetic grain assemblage toward smaller magnetite grains (still larger than SP grains). This change in magnetic grain size is supported by slightly higher ARM/SIRM ratios (**Figure 5L**) in the wet mudflat facies. Dissolution in the water-logged sediment may alter the magnetic grain assemblage and cause poorer remanence preservation and unreliable paleo-directions in the wet mudflat facies.

Hematite dissolution has been observed under reductive conditions (Bloemendal et al., 1993; Liu et al., 2004; Hu et al., 2013), and Yamazaki et al. (2003) found hematite to be more resistive to dissolution than magnetite. The lower HIRM values for the wet mudflat facies (**Figure 5F**) imply the occurrence of partial dissolution of hematite in this facies (**Figure 10**). The steeper slope of the data trend in the HIRM-SIRM-plot at lower SIRM values (**Figure 11A**) supports a higher stability of the hematite fraction compared to magnetite.

SIRM values in **Figure 11A** show a high variability. In principle, the variability could be explained by pronounced variation of detrital input, but this is unlikely the main process (Voigt et al., 2017). Interestingly, the SIRM distribution of specimens with normal polarity directions is shifted to higher SIRM values compared to the specimens with reverse polarity directions (solid curves in **Figure 11A**). Therefore, dissolution of magnetite and hematite grains cannot be the only alteration effect causing secondary magnetizations. The fact that normal polarity samples have higher SIRM values points out the presence of authigenic magnetite that carries a chemical remanent magnetization. Meijers et al. (2016) observed post-depositional partial magnetic overprinting in lacustrine sediments on the Central Anatolian Plateau, associated with removal of primary magnetic grains, neo-formation of magnetite in grayish rocks and precipitation of pigmentary hematite in red and pink clay-rich layers, caused by fluid flow. Magnetite authigenesis may be associated with diagenesis of smectite and illitization (Katz et al., 2000; Tohver et al., 2008). Although much of the illite in the Bastau Fm is of detrital origin (Voigt et al., 2017), pronounced pedogenesis and repeated drying and wetting processes in the wet mudflat facies is highly favorable for slow low-temperature illitization of smectite. The higher NRM/ARM ratio in samples with normal polarity directions compared to the samples with reverse polarity directions (**Figure 11B**) can be explained by authigenic magnetite, which acquired a chemical remanence parallel to the Earth's magnetic field when surpassing the critical grain size (Larson and Walker, 1975). A chemical remanent magnetization of newly formed small magnetite grains is most probably significantly higher than the primary detrital remanent magnetization (Katz et al., 2000). The higher NRM/ARM values are thus interpreted to be indicative for newly formed magnetite (**Figure 10**).

Based on our data, we cannot specify the alteration effect in more detail. However, we can conclude that dissolution and neo-formation of magnetite are likely the key processes in the alteration scenario as indicated by the low concentration dependent parameters in the wet mudflat facies and the higher NRM/ARM ratio in samples with normal polarity directions (**Figure 10**). How and under which conditions the two processes occur in detail, remains an open question that requires further studies.

Because of the interpreted magnetic alteration of the remanence carriers, we suggest to use three criteria (SIRM, HIRM and NRM/ARM ratio) for the selection of the MCC & HCC combined directions, which are less likely affected by (partial) secondary magnetizations. Doing so, one has to notice that the complex interplay and heterogeneity on a small scale compromises the unambiguous identification and selection of samples affected by alteration effects.

Magnetostratigraphy

In order to establish a reliable magnetostratigraphic sequence, we used selection criteria based on the results of remanence analysis and rock magnetic characteristics. Equal area plots of the selections are shown in **Figure 12**.

The results of VGP latitudes along the section based on the HCC only (**Figure 13B**) and the combined MCC & HCC data set (**Figure 13D**) are quite similar (in both plots only specimens meeting the MAD and VGP criteria are included). For further analysis, we use the combined larger data set shown in **Figure 12A** (identical to the one shown in **Figure 4C**). The open circles denoting normal directions within longer intervals of reverse polarity raise issues of the primary origin of these remanences. These remanences mainly correspond to layers of the wet mudflat facies. Since the assignment of the samples into the different facies types is partly difficult (see section Lithofacies Dependence of Rock Magnetic Mineralogy), a general rejection of a facies such as the wet mudflat facies is inappropriate. Thus, in a next step, a selection approach based rock magnetic properties is presented in order to reduce the influence of magnetic alterations and remagnetization.

According to our proposed alteration scenario (**Figure 10**) dissolution and neo-formation of magnetite as well as partial dissolution of hematite caused partial magnetic overprinting in horizons with elevated groundwater availability. Thus, we used rock magnetic properties to identify samples that are likely more affected by secondary magnetization. Based on the assumption that the magnetic alteration caused lower concentration values (SIRM, HIRM) and a higher NRM/ARM ratio (see rock magnetic analyses in section Lithofacies Dependence of Rock Magnetic Mineralogy), samples with the following properties were rejected (**Figures 12B,D**): (1) SIRM $< 1.38 \times 10^{-3}$ Am²/kg below 50 m and SIRM $< 2.53 \times 10^{-3}$ Am²/kg above 50 m; (2) HIRM $< 2.43 \times 10^{-4}$ Am²/kg (3) NRM/ARM > 0.29. The thresholds were determined by median-1σ (SIRM, HIRM) and median $+ 1\sigma$ (NRM/ARM) values. For SIRM two criteria were used for data selection to take into account the higher SIRM values in the upper part of the section. The selection according to NRM/ARM ratios is also in line with the trend of normal and reverse polarity samples shown in **Figure 11B** (i.e., normal polarity samples showing higher NRM/ARM values). The rock magnetic selection criteria remove 93 samples from the MCC & HCC combined data set (**Figures 12B**, **13E**), mostly samples with normal polarity direction (72%) and samples from the wet mudflat facies (56%). Normal polarity samples are suspected to be prime candidates for magnetic overprinting, and thus the higher number of rejected normal polarity samples supports the validity of the rock magnetic selection criteria.

The mean inclination of the reverse polarity directions is $\sim 24^\circ$ lower than the expected Middle Miocene dipole field direction and thus indicate a paleo-remanence influenced by inclination shallowing. Another possible selection approach may employ this interpretation, i.e., the assumption that the reverse polarity directions represent remanences of predominantly primary origin, while normal polarity directions are stronger contaminated by partial secondary magnetization. However, it is difficult to set appropriate criteria for corresponding filtering.

The rock magnetic selection criteria could also be applied to the HCC only. This results in the rejection of 71 samples (179 of 250 samples remaining, see **Figures 12C,D**). Likewise, the selection is effective in reducing the influence of secondary magnetization. The corresponding VGP latitudes in **Figures 13B,C** show a very similar pattern than the MCC & HCC combined data set, with just the reverse polarity interval C5ADr appearing to be shorter. Due to the higher quality and quantity of the MCC & HCC combined data set, we use the MCC & HCC combined result for further interpretations.

With the rock magnetic selection criteria applied to the MCC & HCC combined data set and based on 307 samples, we establish a final magnetostratigraphic sequence, which shows 3 normal and 3 reverse intervals (**Figure 13F**), each interval defined by at least 7 samples. The mean normal direction of all 307 included samples in stratigraphic coordinates is D/I $= 350.3^\circ/53.5^\circ$ ($k = 11.32$, $\alpha_{95} = 2.5^\circ$). We correlate the resulting polarity sequence to the geomagnetic polarity time scale (GPTS) by Gradstein et al. (2012) using the biostratigraphic age of MN4-MN5 (early Miocene, Lucas et al., 2000) at the top of the underlying Aidarly Fm as an anchor. The best match with the reference scale is from the polarity boundary C5Br/C5Bn.2n (15.16 Ma) to the polarity boundary C5ACr/C5ACn (14.07 Ma), as shown in **Figure 13G**.

The sediment accumulation rates (SARs) resulting from this correlation are shown in **Figure 14B** (top). The SAR varies between 3 and 8 cm/ka. Higher SARs occur in intervals where the lithology varies more and coarser grained layers are more pronounced. The mean SAR for the section (6.3 cm/ka) is used to extrapolate the temporal framework of the section at either end.

Out of the 307 samples used to constrain the magnetostratigraphy for the Bastau Fm, 195 are of normal polarity and 112 are of reverse polarity. The mean normal polarity direction is $\sim 19^\circ$ steeper than the mean reverse polarity direction, and the mean declinations differ by $\sim 17^\circ$ from antipodality (**Figure 12B**). Consequently, the reversal test of McFadden and McElhinny (1990) is negative. This indicates still existing unremoved partial magnetic overprinting in the normal polarity directions causing steeper inclinations and declinations tending toward 0° for normal polarity directions (i.e., tending toward the present Earth magnetic field). This effect is known from other continental sedimentary sequences and in the surrounding basins (in the Junggar Basin, Charreau et al., 2005; Subei, Gilder et al., 2001; Tarim Basin, Charreau et al., 2006).

Correlation to the GPTS

The proposed correlation to the GPTS suggests a long reverse interval before the first reversal at the base of the Bastau

Fm. To support this interpretation, we collected additional paleomagnetic samples at the top of the underlying Aidarly Fm (weakly consolidated yellow sandstone). Most layers are much less consolidated and compromise a reliable interpretation. TH and AF demagnetization yielded a complex magnetic behavior with mainly normal polarities. Reverse directions also occur, e.g., from a strongly cemented sandstone layer 7 m below the base of the Bastau Fm. Sandstone is prone to remagnetization and recent overprints, especially weakly consolidated sandstone (Jackson et al., 1993; Kodama, 2012), thus the results from the Aidarly Fm are not considered to be conclusive.

The proposed correlation of the polarity pattern of the Bastau Fm from chron C5B2.2n to chron C5ACr as shown in **Figure 13** results in an age of 15.3–13.9 Ma for the Bastau Fm (ages of the lower and upper ends estimated from linear extrapolation of SARs). The SARs of 3–8 cm/ka (**Figure 14B** top) match well with our field observations of quite continuous sedimentation throughout the section. SAR estimates based on biostratigraphic data are in the range of 5–9 cm/ka and time-series analysis of the Bastau Fm by Voigt et al. (2017) suggests similar SARs. Also, SARs in the range of 6–13 cm/ka were found in other foreland basins of the Tien Shan (Huang et al., 2006; Charreau et al., 2009). An alternative magnetostratigraphic correlation (see **Figure 14A** bottom) matching with the biostratigraphic framework would be between 18 and 16 Ma. However, the resulting SARs show large variation between 2 and 20 cm/ka (**Figure 14B** bottom), and especially the abrupt change to high SAR of 20 cm/ka above the stratigraphic level of 40 m contradicts field observations (Voigt et al., 2017). Other correlations to polarity chrons younger than C5B2.2n-C5ACr principally violates coincidence with the fossil findings from Lucas et al. (2000).

Orbital Control

Orbital forcing of paleoenvironments has been well documented for continental settings (Prokopenko et al., 2006; Vollmer et al., 2008; Abels et al., 2010). Voigt et al. (2017) suggest an orbital control on mudflat deposition in the Bastau Fm. The authors found two dominant cycles in their spectral analysis of geochemical proxies, which they interpret as short (100 ka) and long (405 ka) eccentricity based on its cycle-to-frequency ratio. The Bastau Fm comprises only a small number of 405 ka cycles, the interference of high amplitudes of short eccentricity cycles and minima of long eccentricity causes noisy signals in some intervals, and non-linear feedbacks due to complex interactions of climate and depositional processes have to be taken into account (Hilgen et al., 2015). Although this limits the significance of the cyclostratigraphic interpretation, its principle validity seems reliable. Voigt et al. (2017) suggest the correlation of maxima in the Ti/Al ratio filter outputs to long eccentricity minima (**Figure 15B**). Above the stratigraphic level of 40 m, the correlation is straightforward, whereas below 40 m, i.e., where the depositional variability is the highest, it is more problematic due to the complexity of the signal as described above.

From the spectral analysis of Voigt et al. (2017), we calculated the corresponding SARs, and compared them to the SARs suggested by the magnetostratigraphic correlation (**Figure 15C**). The two curves match well above 40 m but deviate below, i.e., for the lowest (oldest) maxima and minima from the long eccentricity correlation. However, these are the least accurately determined extreme values in the suggested correlation of Voigt et al. (2017). Nevertheless, the SARs are in the same order throughout the section. This supports our interpretation of the magnetic polarity sequence and suggests that the age model developed by our magnetostratigraphic correlation is correct. If the short normal polarity directions within the in the longer reverse intervals in the unfiltered combined data (**Figure 13D**) would be interpreted as valid polarity intervals, the resulting much lower SARs would strongly contradict the SARs obtained from orbital analysis.

With the age model, we can put the succession into the context of the Middle Miocene Climate Transition. Global cooling corresponds with the increasing salinization and the change of magneto-mineralogical properties above 55 m where the lithology changes to saline mudflats and further up to a playa lake.

CONCLUSIONS

The Neogene Aktau Mountains in the Ili Basin, SE Kazakhstan, provide a complex sedimentary record typical for a foreland basin of the Tien Shan Mountains. It is well suited for paleoclimatic research and with the presented magnetostratigraphy may elucidate the role of Central Asia in the Middle Miocene climate evolution. The complex sedimentary setting consists of reddish-colored alluvial floodplain deposits and gray lacustrine deposits. The rocks of the studied sections have been subdivided in three main lithofacies to characterize the depositional variability of the Middle Miocene Bastau Fm (alluvial fan, dry mudflat, and wet mudflat).

Rock magnetic properties of the succession well reflect the depositional variability and allow magnetostratigraphic dating of the Bastau Fm. Stepwise demagnetization revealed a partly complex magnetic behavior with magnetite and hematite as the main magnetic carriers. Thus, detailed rock magnetic analyses were used to analyze the nature of the characteristic remanent magnetization. Remagnetization effects were identified and can be related to intensified evaporative rise of capillary groundwater. The facies dependent remagnetization is best explained by magneto-mineralogical alteration effects, i.e., dissolution of magnetite and hematite and remagnetization due to secondary formed magnetite.

To account for remagnetizations and secondary overprints rock magnetic properties are further used to discriminate remanence directions in order to obtain a reliable magnetostratigraphic result. The presented Middle Miocene magnetostratigraphy provides a robust age model for Bastau Fm with an age from 15.3 to 13.9 Ma.

The age correlation indicates sediment accumulation rates between 3 and 8 cm/ka throughout the section. This is in good agreement with estimates based on biostratigraphic data as well as time-series analysis and corresponds with sedimentation rates found in other foreland basins of the Tien Shan Mountains. Anisotropy of susceptibility results confirm

a detrital sedimentary discharge from the foothills of the Dzhungarian Alatau in the north-west.

Future work should focus on the alteration processes of magnetic minerals, i.e., study authigenic mineral transformations and their effects on remagnetization processes.

AUTHOR CONTRIBUTIONS

All authors substantial contributed to the conception of the work, data acquisition, analysis and interpretation, drafting the work and revising it critically. All gave the final approval of the version to be published and agree to be accountable for all aspects of the work in ensuring that questions related to the accuracy or integrity of any part of the work are appropriately investigated and resolved. VV did the main data acquisition and writing. Analysis, interpretation were mainly done by VV and EA.

ACKNOWLEDGMENTS

This study was financially supported by the Deutsche Forschungsgemeinschaft (DFG grant AP 34/41-1 and VO 687/16-1). We further acknowledge support by the Open Access Publishing Fund of the University Tübingen. Three reviewers helped to improve the manuscript with their constructive comments. We also thank the administration and rangers of the State National Park Altyn Emel for providing access to the Aktau Mountains for geological field work, and Konstantin Kossov and Julia Zhilkina for their support in the field.

REFERENCES

Abels, H., Aziz, H. A., Krijgsman, W., Smeets, S. J. B., and Hilgen, F. J. (2010). Long-period eccentricity control on sedimentary sequences in the continental Madrid Basin (middle Miocene, Spain). *Earth Planet. Sci. Lett.* 289, 220–231. doi: 10.1016/j.epsl.2009.11.011

Bazhanov, V. S., and Kostenko, N. N. (1961). "Geologicheskiy razrez Dzhungarskogo Alatau i ego paleozoologicheskoye obosnovanie [Geological section of Dzhungarian Alatau and its paleontological basis]," in *Materialy po Istorii Fauny i Flory Kazakhstana*, ed I. G. Galuzo (Alma Ata: Akademia Nauk Kazakhskoy SSR), 47–52.

Bloemendal, J., King, J., Hall, F. R., and Doh, S.-J. (1992). Rock magnetism of Late Neogene and Pleistocene deep-sea sediments: relationship to sediment source, diagenetic processes, and sediment lithology. *J. Geophys. Res.* 97, 4361–4375. doi: 10.1029/91JB03068

Bloemendal, J., King, J., Hunt, A., Demenocal, P., and Hayashida, A. (1993). Origin of the sedimentary magnetic record at ocean drilling program sites on the owen ridge, western arabian sea. *J. Geophys. Res.* 98, 4199–4219. doi: 10.1029/92JB02914

Bodina, L. E. (1961). Ostrakody tretichnykh otlozhenii zaisanskoi i iliiskoi depressi [ostracods of tertiary deposits in the zaisan and ili depressions]. *Trudy VNIGRI* 170, 43–153.

Bosboom, R. E., Dupont-Nivet, G., Houben, A. J. P., Brinkhuis, H., Villa, G., Mandic, O., et al. (2011). Late Eocene sea retreat from the Tarim Basin (west China) and concomitant Asian paleoenvironmental change. *Palaeogeogr. Palaeoclimatol. Palaeoecol.* 299, 385–398. doi: 10.1016/j.palaeo.2010.11.019

Bowles, J., Jackson, M., Chen, A., and Solheid, P. (2009). Interpretation of low-temperature data, part 1: Superparamagnetism and paramagnetism. *IRM Quart.* 19. 7–11.

Butler, R.F., (1992) *Paleomagnetism: Magnetic Domains to Geologic Terranes*. Boston, MA: Blackwell Publishing.

Canfield, D. E., and Berner, R. A. (1987). Dissolution and pyritization of magnetite in anoxic marine sediments. *Geochim. Cosmochim. Acta* 51, 645–659. doi: 10.1016/0016-7037(87)90076-7

Caves, J. K., Winnick, M. J., Graham, S. A., Sjostrom, D. J., Mulch, A., and Chamberlain, C. P. (2015). Role of the westerlies in Central Asia climate over the Cenocoic. *Earth Planet. Sci. Lett.* 428, 33–43. doi: 10.1016/j.epsl.2015.07.023

Charreau, J., Chen, Y., Gilder, S., Barrier, L., Dominguez, S., Augier, R., et al. (2009). Neogene uplift of the Tian Shan Mountains observed in the magnetic record of the Jingou River section (northwest China). *Tectonics* 28:TC2008. doi: 10.1029/2007TC002137

Charreau, J., Chen, Y., Gilder, S., Dominguez, S., Avouac, J.-P., Sen, S., et al. (2005). Magnetostratigraphy and rock magnetism of the Neogene Kuitun He section (northwest China): implications for Late Cenozoic uplift of the Tianshan mountains, *Earth Planet. Sci. Lett.* 230, 177–192. doi: 10.1016/j.epsl.2004.11.002

Charreau, J., Gilder, S., Chen, Y., Dominguez, S., Avouac, J.-P., Sen, S., et al. (2006). Magnetostratigraphy of the Yaha section, Tarim Basin (China): 11 Ma acceleration in erosion and uplift of the Tian Shan mountains. *Geology* 34, 181–184. doi: 10.1130/G22106.1

Demory, F., Oberhänsli, H., Nowaczyk, N. R., Gottschalk, M., Wirth, R., and Naumann, R. (2005). Detrital input and early diagenesis in sediments from Lake Baikal revealed by rock magnetism. *Glob. Planet. Change* 46, 145–166. doi: 10.1016/j.gloplacha.2004.11.010

Deng, C. L., Liu, Q. S., Wang, W., and Liu, C. C. (2007). Chemical overprint on the natural remanent magnetization of a subtropical red soil sequence in the Bose Basin, southern China. *Geophys. Res. Lett.* 34:L22308. doi: 10.1029/2007GL031400

Deocampo, D. M. (2015). Authigenic clay minerals in lacustrine mudstones. *Geol. Soc. Am. Spec. Paper*. 515, 45–64. doi: 10.1130/2015.2515(03)

Dzhamangaraeva, A. K. (1997). Pliocene charophytes from Aktau Mountain, southeastern Kazakhstan. *Geobios* 30, 475–479. doi: 10.1016/S0016-6995(97)80115-5

Felletti, F., Dall'Olio, E., and Muttoni, G. (2016). Determining flow directions in turbidites: an integrated sedimentological and magnetic fabric study of the Miocene Marnoso Arenacea Formation (northern Apennines, Italy). *Sediment. Geol.* 335, 197–215. doi: 10.1016/j.sedgeo.2016.02.009

Fisher, R. A. (1953). Dispersion on a sphere. *Proc. R. Soc. Lond. A* 217, 295–302. doi: 10.1098/rspa.1953.0064

Florindo, F., Roberts, A., and Palmer, M. R. (2003). Magnetite dissolution in siliceous sediments. *Geochem. Geophys. Geosyst.* 4:1053. doi: 10.1029/2003GC000516

Fluteau, F., Ramstein, G., and Besse, J. (1999). Simulating the evolution of the Asian and African monsoons during the past 30 Myr using an atmospheric general circulation model. *J. Geophys. Res.* 104, 11995–12018. doi: 10.1029/1999JD900048

Gale, A. S., Huggett, J. M., Pälike, H., Laurie, E., Hailwood, E. A., and Hardenbol, J. (2006). Correlation of Eocene-Oligocene marine and continental records: orbital cyclicity, magnetostratigraphy and sequence stratigraphy of the Solent Group, Isle of Wight, UK. *J. Geol. Soc. Lond.* 163, 401–415. doi: 10.1144/0016-764903-175

Gilder, S., Chen, Y., and Sen, S. (2001). Oligo-Miocene magnetostratigraphy and rock magnetism of the Xishuigou section, Subei (Gansu Province, western China) and implications for shallow inclinations in central Asia. *J. Geophys. Res.* 106, 30505–30521. doi: 10.1029/2001JB000325

Gradstein, F. M., Ogg, J. G., Schmitz, M., and Ogg, G. (2012). *The Geologic Time Scale 2012*. Boston, MA: Elsevier B.V.

Guo, Z. T., Ruddiman, W. F., Hao, Q. Z., Wu, H. B., Qiao, Y. S., Zhu, R. X., et al. (2002). Onset of Asian desertification by 22 Myr ago inferred from loess deposits in China. *Nature* 416, 159–163. doi: 10.1038/416159a

Hays, J. D., Imbrie, J., and Shackleton, N. J. (1976). Variations in the Earth's orbit: pacemaker of the ice ages. *Science* 194, 1121–1132. doi: 10.1126/science.194.4270.1121

Herb, C., Appel, E., Voigt, S., Koutsodendris, A., Pross, J., Zhang, W., et al. (2015). Orbitally tuned age model for the late Pliocene–Pleistocene lacustrine

succession of drill core SG-1 from the western Qaidam Basin (NE Tibetan Plateau). *Geophys. J. Int*. 200, 35–51. doi: 10.1093/gji/ggu372

Hilgen, F. J., Hinnov, L. A., Abdul Aziz, H., Abels, H. A., Batenburg, S., Bosmans, J. H. C., et al. (2015). Stratigraphic continuity and fragmentary sedimentation: the success of cyclostratigraphy as part of integrated stratigraphy. *Geol. Soc. Lond. Spec. Publ.* 404, 157–197. doi: 10.1144/SP404.12

Hounslow, M. W., and Nawrocki, J. (2008). Palaeomagnetism and magnetostratigraphy of the Permian and Triassic of Spitsbergen: a review of progress and challenges. *Polar Res.* 27, 502–522. doi: 10.1111/j.1751-8369.2008.00075.x

Hu, P., Liu, Q., Torrent, J., Barrón, V., and Jin, C. (2013). Characterizing and quantifying iron oxides in Chinese loess/paleosols: implications for pedogenesis. *Earth Planet. Sci. Lett*. 369-370, 271–283. doi: 10.1016/j.epsl.2013.03.033

Hu, S. Y., Goddu, S. R., Appel, E., Verosub, K., Yang, X. D., and Wang, S. M. (2005). Palaeoclimatic changes over past one million years derived from lacustrine sediments of Heqing Basin (Yunnan, China). *Quatern. Int*. 136, 123–129. doi: 10.1016/j.quaint.2004.11.013

Hu, S. Y., Goddu, S. R., Herb, C., Appel, E., Gleixner, G., Wang, S. M., et al. (2015). Climate variability and its magnetic response recorded in a lacustrine sequence in Heqing basin at the SE Tibetan Plateau since 900 ka. *Geophys. J. Int*. 201, 444–458. doi: 10.1093/gji/ggv033

Huang, B. C., Piper, J. D. A., Peng, S. T., Liu, T., Li, Z., Wang, Q. C., et al. (2006). Magnetostratigraphic study of the Kuche Depression, Tarim Basin, and Cenozoic uplift of the Tian Shan Range, Western China. *Earth Planet. Sci. Lett*. 251, 346–364. doi: 10.1016/j.epsl.2006.09.020

Itoh, Y., Tamaki, M., and Takano, O. (2013). "Rock Magnetic Properties of Sedimentary Rocks in Central Hokkaido - Insights into Sedimentary and Tectonic Processes on an Active Margin," in *Mechanism of Sedimentary Basin Formation - Multidisciplinary Approach on Active Plate Margins*, ed Y. Itoh (Rijeka: InTech), 233–253.

Jackson, M., Borradaile, G., Hudleston, P., and Banerjee, S. (1993). Experimental deformation of synthetic magnetite-bearing calcite sandstones: effects on remanence, bulk magnetic properties, and magnetic anisotropy. *J. Geophys. Res.* 98, 383–401. doi: 10.1029/92JB01028

Jelinek, V. (1981). Characterization of the magnetic fabrics of rocks. *Tectonophysics* 79, 63–67. doi: 10.1016/0040-1951(81)90110-4

Jolivet, M., Dominguez, S., Charreau, J., Chen, Y., Li, Y., and Wang, Q. (2010). Mesozoic and Cenozoic tectonic history of the central Chinese Tian Shan: Reactivated tectonic structures and active deformation. *Tectonics* 29:TC6019. doi: 10.1029/2010TC002712

Jordanova, N. (2016). *Soil Magnetism: Applications in Pedology, Environmental Science and Agriculture*. Academic Press.

Karlin, R., and Levi, S. (1985). Geochemical and sedimentological control of the magnetic properties of hemipelagic sediments. *J. Geophys. Res*. 90, 10373–10392. doi: 10.1029/JB090iB12p10373

Katz, B., Elmore, R. D., Cogoini, M., Engel, M. H., and Ferry, S. (2000). Associations between burial diagenesis of smectite, chemical remagnetization, and magnetite authigenesis in the Vocontian trough, SE France. *J. Geophys. Res.* 105, 851–868. doi: 10.1029/1999JB900309

Kirschvink, J. L. (1980). The least squares line and plane and the analysis of paleomagnetic data. *Geophys. J. R. Astron. Soc*. 62, 699–712. doi: 10.1111/j.1365-246X.1980.tb02601.x

Kodama, K. P. (2012). *Paleomagnetism of Sedimentary Rocks: Process and Interpretation*. Oxford: Wiley-Blackwell.

Kodama, K. P., and Hinnov, L. A. (2015). *Rock magnetic cyclostratigraphy*. Oxford: Wiley-Blackwell.

Kordikova, E. G. (2000). Insectivora (Mammalia) from the Lower Miocene of the Aktau Mountains, South-Eastern Kazakhstan. *Senckenb. Lethaea* 80, 67–79. doi: 10.1007/BF03043665

Kordikova, E. G., and de Bruijn, H. (2001). Early Miocene Rodents from the Aktau Mountains (South-Eastern Kazakhstan). *Senckenb. Lethaea* 81, 391–405. doi: 10.1007/BF03042791

Kordikova, E. G., and Mavrin, A. V. (1996). Stratigraphy and Oligocene-Miocene mammalian biochronology of the Aktau Mountains, Dzhungarian Alatau range, Kazakhstan. *Palaeovertebrata* 25, 141–174.

Krijgsman, W., Delahaije, W., Langreis, C., and de Boer, P. L. (1999). Paleomagnetism and astronomically induced cyclicity of the Armantes section; a Miocene continental red sequence in the Calatayud-Daroca basin (Central Spain). *Acta Geol. Hispanica* 32, 201–219.

Krijgsman, W., Hilgen, F. J., Langereis, C., Santarelli, A., and Zachariasse, W. J. (1995). Late Miocene magnetostratigraphy, biostratigraphy and cyclostratigraphy in the Mediterranean. *Earth Planet. Sci. Lett.* 136, 475–494. doi: 10.1016/0012-821X(95)00206-R

Kruiver, P. P., Dekkers, M. J., and Heslop, D. (2001). Quantification of magnetic coercivity by the analysis of acquisition curves of isothermal remanent magnetisation. *Earth Planet. Sci. Lett.* 189, 269–276. doi: 10.1016/S0012-821X(01)00367-3

Kruiver, P. P., Langreis, C. G., Dekker, M. J., and Krijgsman, W. (2003). Rock-magnetic properties of multicomponent natural remanent magnetization in alluvial red beds (NE Spain). *Geophys. J. Int*. 153, 317–332. doi: 10.1046/j.1365-246X.2003.01880.x

Larson, E. D., and Walker, T. R. (1975). Development of chemical remanent magnetization during early stages of red-bed formation in Late Cenozoic sediments, Baja, California. *Geol. Soc. Am. Bull.* 86, 639–650. doi: 10.1130/0016-7606(1975)86<639:DOCRMD>2.0.CO;2

Liu, J., Zhu, R., Roberts, A., Li, S., and Chang, J. (2004). High-resolution analysis of early diagenetic effects on magnetic minerals in post-middle-Holocene continental shelf sediments from the Korea Strait. *J. Geophys. Res.* 109:B03103. doi: 10.1029/2003JB002813

Lu, H., Wang, X., and Li, L. (2010). "Aeolian sediment evidence that global cooling has driven late Cenozoic stepwise aridification in central Asia," in *Monsoon Evolution and Tectonics-Climate Linkage in Asia.* ed P. D. Clift, R. Tada, and H. Zheng (Geological Society, Special Publications), 29–44.

Lucas, S. G., Aubekerov, B. Z., Dzhamangaraeva, A. K., Bayshashov, B. U., and Tyutkova, L. A. (2000). "Cenozoic lacustrine deposits of the Ili basin, southeastern Kazakhstan," in *Lake Basins Through Space and Time,* ed E. Gierlowski-Kordesch, K. R. Kelts (AAPG Studies in Geology), 59–64.

Lucas, S. G., Bayshashov, B. U., Tyutkova, L. A., Zhamangara, A. K., and Aubekerov, B. Z. (1997). Mammalian biochronology of the Paleogene-Neogene boundary at Aktau Mountain, eastern Kazakhstan. *Paläontol. Z.* 71, 305–314. doi: 10.1007/BF02988498

McCabe, C., and Elmore, R. D. (1989). The occurrence and origin of Late Paleozoic remagnetization in the sedimentary rocks of North America. *Rev. Geophys.* 27, 471–493. doi: 10.1029/RG027i004p00471

McFadden, P. L., and McElhinny, M. W. (1990). Classification of the reversal test in paleomagnetism. *Geophys. J. Int*. 130, 725–729. doi: 10.1111/j.1365-246X.1990.tb05683.x

Meijers, M. J. M., Strauss, B. E., Özkaptan, M., Feinberg, J. M., Mulch, A., and Whitney, D. L., Kaymakci, N. (2016). Age and paleoenvironmental reconstruction of partially remagnetized lacustrine sedimentary rocks (Oligocene Aktoprak basin, central Anatolia, Turkey). *Geochem. Geophys. Geosyst*. 17, 914–939. doi: 10.1002/2015GC006209

Miao,Y., Herrmann, M., Wu, F., and Yan, X., Yang, S. (2012). What controlled Mid–Late Miocene long-term aridification in Central Asia? - Global cooling or Tibetan Plateau uplift: a review. *Earth Sci. Rev.* 112, 155–172. doi: 10.1016/j.earscirev.2012.02.003

Olsen, P. E., and Kent, D. V. (1996). Milankovitch climate forcing in the tropics of Pangea during the Late Triassic. *Palaeogeogr. Palaeoclimatol. Palaeoecol.* 122, 1–26. doi: 10.1016/0031-0182(95)00171-9

Prokopenko, A. A., Hinnov, L., Williams, D. F., and Kuzmin, M. I. (2006). Orbital forcing of continental climate during the Pleistocene: a complete astronomically tuned climatic record from Lake Baikal, SE Siberia. *Quat. Sci. Rev.* 25, 3431–3457. doi: 10.1016/j.quascirev.2006.10.002

Roberts, A. P. (2015). Magnetic mineral diagenesis. *Earth Sci. Rev.* 151, 1–47. doi: 10.1016/j.earscirev.2015.09.010

Roberts, A. P., Florindo, F., Larrasoaña, J. C., O'Regan, M. A., and Zhao, X. (2010). Complex polarity pattern at the former Plio–Pleistocene global stratotype section at Vrica (Italy): remagnetization by magnetic iron sulfides. *Earth Planet. Sci. Lett.* 292, 98–111. doi: 10.1016/j.epsl.2010.01.025

Roberts, A. P., Tauxe, L., and Heslop, D. (2013). Magnetic paleointensity stratigraphy and high-resolution Quaternary geochronology: successes and future challenges. *Quat. Sci. Rev.* 61, 1–16. doi: 10.1016/j.quascirev.2012.10.036

Sun, M., Zhang, X., Tian, M., Liu, R., He, Z., Qi, L., et al. (2017). Loess deposits since early Pleistocene in northeast China and implications for desert evolution in east China. *J. Asian Earth Sci*. 155, 164-173. doi: 10.1016/j.jseaes.2017.09.013

Tang, Z., Ding, Z., White, P. D., Dong, X., Ji, J., Jiang, H., et al. (2011). Late Cenozoic central Asian drying inferred from a palynological record from the northern Tian Shan. *Earth Planet. Sci. Lett.* 302, 439–447. doi: 10.1016/j.epsl.2010.12.042

Tang, Z., Huang, B., Dong, X., Ji, J., and Ding, Z. (2012). Anisotropy of magnetic susceptibility of the Jingou River section: Implications for late Cenozoic uplift of the Tian Shan. *Geochem., Geophys. Geosyst*. 13:Q03022. doi: 10.1029/2011GC003966

Tarling, D. H., and Hrouda, F. (1993). *The Magnetic Anisotropy of Rocks.* London: Chapman & Hall.

Tauxe, L., and Kent, D. V. (1984). Properties of a detrital remanence carried by haematite from study of modern river deposits and laboratory redeposition experiments. *Geophys. J. R. Astr. Soc.* 77, 543–561. doi: 10.1111/j.1365-246X.1984.tb01909.x

Tauxe, L., Kent, D. V., and Opdyke, N. D. (1980). Magnetic components contributing to the NRM of Middle Siwalik red beds. *Earth Planet. Sci. Lett.* 47, 279–284. doi: 10.1016/0012-821X(80)90044-8

Taylor, S. N., Lagroix, F., Rousseau, D.-D., and Antoine, P. (2014). Mineral magnetic characterization of the Upper Pleniglacial Nussloch loess sequence (Germany): an insight into local environmental processes. *Geophys. J. Int*. 199, 1463–1480. doi: 10.1093/gji/ggu331

Tohver, E., Weil, A. B., Solum, J. G., and Hall, C. M. (2008). Direct dating of carbonate remagnetization by $^{40}Ar/^{39}Ar$ analysis of the smectite–illite transformation. *Earth Planet. Sci. Lett*. 274, 524–530. doi: 10.1016/j.epsl.2008.08.002

Torsvik, T. H., van der Voo, R., Preeden, U., Mac Niocaill, C., Steinberger, B., Doubrovine, P. V., et al. (2012). Phanerozoic polar wander, palaeogeography and dynamics. *Earth Sci. Rev*. 114, 325–368. doi: 10.1016/j.earscirev.2012.06.007

van der Voo, R., and Torsvik, T. H. (2012). "The history of remagnetization of sedimentary rocks: deceptions, developments and discoveries," in *Remagnetization and Chemical Alteration of Sedimentary Rocks*, eds R. D. Elmore, A. R. Muxworthy, M. Aldana, and M. Mena (Geological Society, London, Special Publications), 23–53

Voigt, S., Weber, Y., Frisch, K., Bartenstein, A., Hellwig, A., Petschick, R., et al. (2017). Climatically forced moisture supply, sediment flux and pedogenesis in Miocene mudflat deposits of south-east Kazakhstan, Central Asia. *Deposit. Rec.* 3, 209–232. doi: 10.1002/dep2.34

Vollmer, T., Werner, R., Weber, M., Tougiannidis, N., Röhling, H.-G., and Hambach, U. (2008). Orbital control on Upper Triassic Playa cycles of the Steinmergel-Keuper (Norian): a new concept for ancient playa cycles. *Palaeogeogr. Palaeoclimatol. Palaeoecol.* 267, 1–16. doi: 10.1016/j.palaeo.2007.12.017

Yamazaki, T., Abdeldayem, A., and Ikehara, K. (2003). Rock-magnetic changes with reduction diagenesis in Japan Sea sediments and preservation of geomagnetic secular variation in inclination during the last 30,000 years. *Earth Planets Space* 55, 327–340. doi: 10.1186/BF03351766

Zhang, C., Paterson, G. A., and Liu, Q. (2012). A new mechanism for the magnetic enhancement of hematite during heating: the role of clay minerals. *Stud. Geophys. Geod*. 56, 845–860. doi: 10.1007/s11200-011-9018-4

Zhang, W. L., Appel, E., Fang, X. M., Yan, M. D., Song, C. H., and Cao, L. W. (2012). Paleoclimatic implications of magnetic susceptibility in Late Pliocene-Quaternary sediments from deep drilling core SG-1 in the western Qaidam Basin (NE Tibetan Plateau). *J. Geophys. Res.* 117:B06101. doi: 10.1029/2011JB008949

Zhisheng, A., Kutzbach, J. E., Prell, W. L., and Porter, S. C. (2001). Evolution of Asian monsoons and phased uplift of the Himalaya-Tibetan Plateau since late Miocene times. *Nature* 411, 62–66. doi: 10.1038/35075035

Conflict of Interest Statement: The authors declare that the research was conducted in the absence of any commercial or financial relationships that could be construed as a potential conflict of interest.